Observed Processes Underlying the Favorable Vortex Repositioning Early in the Development of Hurricane Dorian (2019)

GEORGE R. ALVEY III,[a,b] MICHAEL FISCHER,[a,b] PAUL REASOR,[b] JONATHAN ZAWISLAK,[a,b] AND ROBERT ROGERS[b]

[a] *Cooperative Institute for Marine and Atmospheric Studies, University of Miami, Miami, Florida*
[b] *NOAA/Atlantic Oceanographic and Meteorological Laboratory/Hurricane Research Division, Miami, Florida*

(Manuscript received 2 April 2021, in final form 9 July 2021)

ABSTRACT: Dorian's evolution from a weak, disorganized tropical storm to a rapidly intensifying hurricane is documented through a unique multiplatform synthesis of NOAA's P-3 tail-Doppler radar, airborne in situ data, and Météo-France's Martinique and Guadeloupe ground radar network. Dorian initially struggled to intensify with a misaligned vortex in moderate midtropospheric vertical wind shear that also allowed detrimental impacts from dry air near the inner core. Despite vertical wind shear eventually decreasing to less than 5 m s^{-1} and an increasingly symmetric distribution of stratiform precipitation, the vortex maintained its misalignment with asymmetric convection for 12 h. Then, as the low-level circulation (LLC) approached St. Lucia, deep convection near the LLC center dissipated, the LLC broadened, and precipitation expanded radially outward from the center temporally coinciding with the diurnal cycle. Convection then developed farther downtilt within a more favorable, humid environment and deepened appreciably at least partially due to interaction with Martinique. A distinct repositioning of the LLC toward Martinique was induced by a spinup of a mesovortex into a small, compact LLC. It is hypothesized that this somewhat atypical reformation event and the repositioning of the vortex into a more favorable environment, farther from detrimental dry midtropospheric air, increased its favorability for the rapid intensification that subsequently ensued. Although the repositioning resulted in tilt reducing to less than the scale of the vortex itself, the preexisting broad mid- to upper-level cyclonic envelope remained intact with continued misalignment observed between the midlevel center and repositioned LLC even during the early stages of rapid intensification.

KEYWORDS: Atlantic Ocean; Convective clouds; Hurricanes/typhoons; Precipitation; Tropical cyclones; Vortices; Clouds; Mesoscale processes; Mesoscale systems; Vorticity; Aircraft observations; Radars/Radar observations; Operational forecasting

1. Introduction

Intensity forecast skill has benefited from advancements in numerical weather prediction (NWP), improved statistical guidance, and an increased fundamental understanding of TC processes (Cangialosi et al. 2020). Despite some gradual improvements in TC intensity change prediction in recent years, more work is still needed to match the improvement seen in track forecasts (DeMaria et al. 2014; Cangialosi et al. 2020), particularly for rapid intensification (RI). More than 70% of all rapid intensity change events begin as weak TCs [≤ 50 kt (1 kt ≈ 0.51 m s^{-1}),Wang and Jiang 2021, cf. their Fig. 6], often during early stage development periods with considerable predictability issues. Further complicating matters, even those TCs within marginally favorable environments (e.g., moderate vertical wind shear and dry midtropospheric air; Rios-Berrios et al. 2016; Munsell et al. 2017; Alvey et al. 2020) can undergo RI. Poor predictability in these scenarios is attributed to a variety of factors including insufficient model representation of initial conditions, inadequate representations of complex multifaceted interactions within both the inner core and surrounding environment, and incomplete understanding of intensification processes in weak TCs (Zhang and Tao 2013).

One important environmental process that plays a large role in TC intensification (DeMaria and Kaplan 1994), vertical wind shear, can detrimentally ventilate the warm core (Frank and Ritchie 2001; Tang and Emanuel 2010, 2012) and differentially advect the upright potential vorticity into a more tilted, or misaligned, configuration. Although azimuthal asymmetries in precipitation and heating (Jones 2000; Reasor et al. 2004; Hence and Houze 2011) induced by a tilted vortex alone do not make a TC unfavorable for intensification, heating displaced well away from the surface center of circulation would be expected to spin up the mean tangential winds less effectively than comparable heating near the rotation axis (Schubert and Hack 1982). Furthermore, a misaligned vortex increases susceptibility of the TC to entrainment of drier environmental air. Dry air not only dilutes convective updrafts but can also entrain into convective downdrafts that flush the boundary layer with unfavorable, low θ_e air (Riemer et al. 2010; Finocchio et al. 2016; Nguyen et al. 2017, 2019; Chen et al. 2019; Alland et al. 2021a).

Because a misaligned structure can cause unfavorable effects that hinder TC intensification and make a TC susceptible to further increases in tilt, it is important to understand how a vortex becomes nearly vertically aligned, a characteristic identified near RI onset (e.g., Leighton et al. 2018; Alvey et al. 2020; Rogers et al. 2020) in most TCs. Some studies have shown that the mid- to upper-level vortex precesses into the upshear quadrants preceding alignment (Jones 1995;

Corresponding author: George R. Alvey, george.alvey@noaa.gov

DOI: 10.1175/MWR-D-21-0069.1

Finocchio et al. 2016; Munsell et al. 2017); however, they tend to focus on more developed, coherent vortices found in numerical simulations of stronger tropical storms (≥50 kt). On the other hand, persistent deep convection located near the misaligned midlevel circulation (MLC) can actually lead to the development of a new low-level circulation (LLC) through a pathway commonly referred to as *downshear reformation* (Nguyen and Molinari 2015; Chen et al. 2018; Rogers et al. 2020). Using an ensemble of forecasts of Edouard (2014), Alvey et al. (2020) showed that members achieved alignment through separate pathways: precession, reformation, and vorticity advective processes.[1] The culmination of the transition from asymmetric toward symmetric precipitation, associated thermodynamic changes, and vortex merger processes that result in an aligned vortex is referred to as restructuring (Rios-Berrios et al. 2018). All of the aforementioned modeling and case studies featured persistent, moderate to strong vertical wind shear. The question then becomes; what processes most directly contribute toward alignment in an environment with decreasing vertical wind shear?

Using a series of idealized simulations that smoothly transitioned vertical wind shear from higher, more unfavorable magnitudes to lesser, more favorable magnitudes, Onderlinde and Nolan (2017) found a time-lagged response in the vortex structure as it maintained a residual footprint from the initial higher shear environment. A recent modeling study by Schecter and Menelaou (2020) invoked a technique, whereby misalignment was induced and subsequently examined in an environment without vertical wind shear. For initial misalignments greatly exceeding the radial length scale of the vortex, a state of vertical alignment was ultimately achieved as the surface center migrated toward a convective complex and attendant MLC. Diabatic processes were critical to the complete alignment as confluent flow advected the surface center toward the convection and mixing of diabatically generated vortices and filaments reshaped the surface circulation. At earlier stages of the tilt evolution, however, a period of rapid reduction in misalignment coinciding with midtropospheric vortex reformation was followed by substantial regrowth of misalignment via adiabatic mechanisms, highlighting the general complexity of the dynamics governing even nonsheared restructuring of early-stage TCs. Emphasizing the importance of the tilt magnitude, Schecter and Menelaou observed a strong correlation between the time required to intensify from an incipient TC to a hurricane and the time-averaged tilt over that period.

Dorian (2019), a historic storm with significant impacts (Avila et al. 2020), featured notable predictability issues during its early stages surrounding a restructuring event that involved interactions with the Windward Islands. Because Dorian's alignment also occurred in a decreasing shear environment, Onderlinde and Nolan (2017) and Schecter and Menelaou (2020) provide context from modeling perspectives that will be compared to Dorian's observations.

To fully capture events that occur on relatively short convective time scales, a combination of preexisting and novel techniques is used to leverage both airborne and ground-based observing platforms. This facilitates analysis of interactions between large-scale and vortex-scale processes through increased spatial coverage and high temporal resolution. In particular, both ground radar and airborne radar provide a synthesized analysis during the poorly predicted vortex restructuring period, in which Dorian transitions from a misaligned, asymmetric tropical storm to a relatively aligned, rapidly intensifying TC.

This study addresses the following questions within this early intensification period of Dorian: What multiscale changes preceded the near-complete alignment of Dorian? How can alignment be better anticipated in order to improve prediction? First, we assess the environmental context for the restructuring and then examine the processes responsible for the surface and midlevel vortex evolution that ends in sufficient alignment for RI to occur. A unique phenomenon is identified wherein island enhancement of convection is believed to aid the reformation of the LLC. Finally, it will be shown how Dorian's center repositioning preconditioned it for RI.

2. Overview and motivation

a. *Synopsis*

The NHC classified a tropical wave originating off the coast of Africa as a tropical depression in the central Atlantic on 0600 UTC 24 August (Avila et al. 2020). From 24 to 27 August, the poorly organized tropical cyclone struggled to intensify, even after being upgraded to Tropical Storm Dorian. The NHC forecasters attributed the lack of organization to the possibility of dry air intrusions (Avila et al. 2020). Around 1200 UTC 27 August, the LLC became difficult to locate in real-time operations following its disruption near St. Lucia (Stewart 2019). The NHC's postanalysis TC report states that "the high mountains of (St. Lucia) disrupted the organization of the cyclone's LLC, and the center then reformed to the north … " resulting, "in a significant shift in track."

This study focuses on the series of events surrounding this vortex repositioning because it is hypothesized to be a critical event in Dorian's RI preconditioning, and likely also contributed significantly to the poor track and intensity forecasts of Dorian in the eastern Caribbean. Figure 1a (subpanel) shows that the NHC's best track (black X marks) does not capture the vortex repositioning (red line) that represents a fairly significant jump in the LLC's track by greater than 50 km. Therefore, events are temporally referenced in this study with respect to this repositioning time, defined as 0 h on 1200 UTC 27 August (Figs. 1a,c). The time chosen represents the authors' best interpretation accurate to within 1–2 h when the newly repositioned LLC becomes a trackable feature with Martinique's ground radar.

[1] Vorticity maxima were observed to partially rotate around the anchored, broad preexisting cyclonic envelope before aggregating in several members.

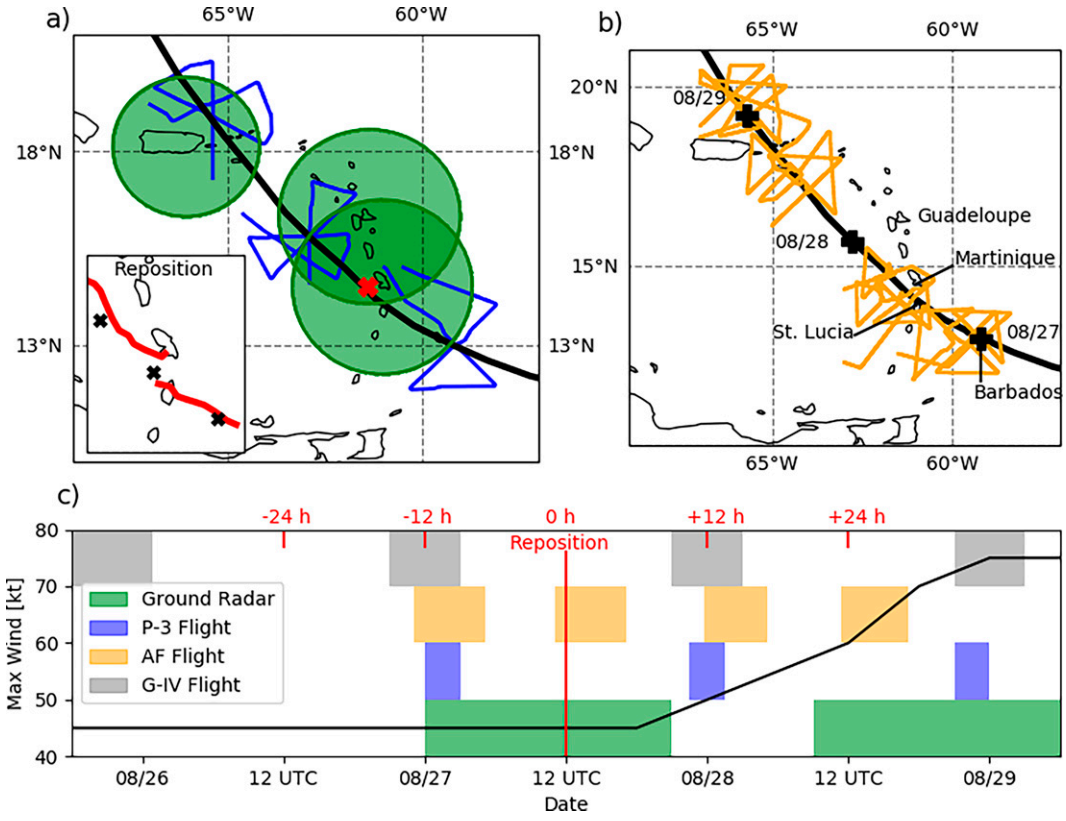

FIG. 1. (a) The best track (black line), NOAA P-3 flight tracks (blue lines), and ground radar coverages (green shading). The red X marks the repositioning time, denoted in (a). The embedded subpanel in (a) shows a zoomed in view of the vortex repositioning with best track (black X) and ground radar determined low-level center tracks (red lines). (b) The NHC best track (black line) and Air Force flight tracks (orange) with 24-h periods marked (+). (c) The NHC best track intensity (maximum sustained winds, black line) with ground radar observation periods (Martinique, Guadeloupe, Puerto Rico) outlined by green shading. NOAA P-3 (blue shading), G-IV (gray shading), and Air Force (orange shading) flights are also plotted in (c). The red line denotes the approximate time of vortex repositioning and times are indicated with respect to that period.

After repositioning, Dorian moved more toward the NW and began to rapidly intensify[2] (25 kt in 24 h) at 1800 UTC 27 August, 6 h after repositioning (Fig. 1c). Dorian eventually formed a partial eyewall on 28 August and intensified into a 75-kt hurricane just northeast of Puerto Rico.

b. *Motivation*

Numerical models consistently struggled to capture Dorian's track and intensity during the period from 26 to 28 August (Hazelton et al. 2021). Intensity forecasts issued on 26 August (Fig. 2a) initially over predicted intensification by 10–20 kt. In several subsequent cycles, model guidance tracked Dorian too far toward the west (Fig. 2b) with track errors exceeding the climatological average in short and medium ranges (Avila et al. 2020). Finally, the inability of model guidance and forecasts to capture a period of RI on 28 August (Fig. 2a) is a key motivating factor and likely also contributed to the large track errors (Hazelton et al. 2021).

c. *Observing platform timeline*

Dorian was well observed by both airborne and ground based platforms from 26 to 29 August with three NOAA P-3 flights during that period (Figs. 1a,c). In situ flight level (~3-km or 700-hPa altitude) wind, extrapolated surface pressure, and dropsonde data from the P-3 flights provide kinematic and thermodynamic measurements. Four Air Force Reconnaissance flights (Figs. 1b,c) at ~1.5 km (850 hPa) altitude also provide in situ flight level measurements. Three G-IV missions flew at altitudes of ~13–14 km (200–150 hPa) between 25 and 28 August (Fig. 1c). Ground radars operated by Météo-France from Martinique and Guadeloupe (Figs. 1a,c) are a key component of this study, as their analyses importantly fill radar gaps between the once daily P-3 flights on 27–28 August. Section 3 provides additional details about the observing platforms and data retrieval techniques.

[2] Kaplan and DeMaria (2003) first defined rapid intensification as a 30-kt intensity change in 24 h. More recently, however, 25 kt in 24 h has also been adopted as an indicator of RI (Kaplan et al. 2010).

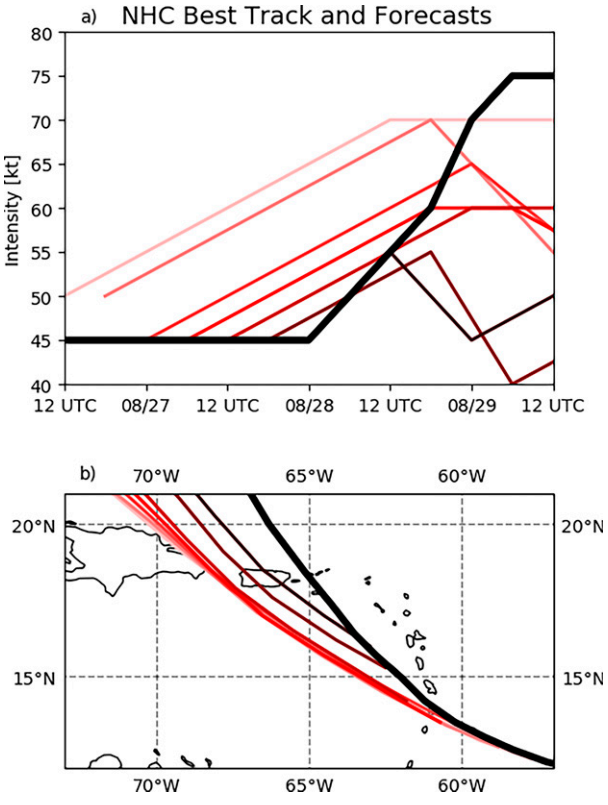

FIG. 2. NHC official (a) intensity and (b) track forecasts issued from 1200 UTC 26 Aug to 0000 UTC 28 Aug (progressing from lighter shading red lines to darker red lines). Bold black line is the NHC's best track.

3. Methodologies

The P-3's fore- and aft-scanning tail-Doppler radar (TDR) allows for three-dimensional wind and reflectivity analyses following methodologies described in Gamache (1997) and Reasor et al. (2009). Analyses of the kinematic structure of the TC within swaths along the flight track are generated for each radial penetration through the TC center. Observations from the X-band radar extend out as far as 50 km on either side of the flight track. Radar observations from each center pass during a specific flight are composited to create a "merged" analysis, which yields a greater azimuthal coverage of the kinematic structure of the vortex (Rogers et al. 2012, 2013; Reasor et al. 2013). Prior to the compositing, each radial flight leg with TDR observations undergoes a recentering process, where the TC center is determined to be the location that maximizes the tangential component of the motion-relative vortex flow on a spatial scale comparable to the TC's RMW (Fischer et al. 2021).

Center tracks during the periods of ground-based radar observation are determined for the low levels (0–2-km layer mean) and midlevels (4–6-km layer mean) using constant altitude plan position indicators (CAPPIs). The CAPPIs are constructed by interpolating elevation angle scans of the radial velocity (and reflectivity) from the Martinique and Guadeloupe ground radars into 0.5-km vertically (2-km horizontal resolution) spaced Cartesian grids. Additional details regarding the ground radars used in this study can be found in Table 1. Although objective center tracking using the modified ground-based velocity track display (GBVTD) algorithm (Lee et al. 1999) was attempted, a center analysis using a modified version of the linear least squares derivative (LLSD) azimuthal shear (Smith and Elmore 2004) with the addition of *K*-means clustering proved more robust for this case, likely due to Dorian's weaker intensity. Because individual convective elements create a large amount of noise, centers were determined for two scales: the higher resolution convective scale with a 3 × 3 gridded median filter (~6-km resolution) and a coarser 25 × 25 grid median filter (~50 km resolution) to capture the mesoscale parent circulations. It is also important to note that the centers are more difficult to track within ~50 km of Martinique's radar, and therefore also require some subjective interpretation with significant input from Guadeloupe's radial velocity. Unless otherwise specified, ground radar centers utilize the coarser median filter and radii of maximum winds[3] (RMWs) use the high-resolution filter.

Following methodologies from Alvey et al. (2020) and Rogers et al. (2020), the ground radar CAPPI's are also used to delineate precipitation types based on a modified Steiner et al. (1995) algorithm. Precipitation is first categorized as convection, stratiform, or anvil using radar reflectivity thresholds outlined in Alvey et al. (2020). Those pixels that are convective are then classified based on the maximum heights of the 20-dB*Z* echo: shallow (0–6 km), moderate (6–10), and deep (>10 km). Convection with a 25-dB*Z* echo height greater than 8 km is also classified as deep convection; this additional stratification is applied for those areas within the CAPPIs that have limited data above 10 km due to beam angle constraints. Importantly, compositing the Guadeloupe and Martinique radars provides additional mid- to upper-atmospheric elevation angles overhead their counterparts, where the lack of elevation scans would traditionally limit coverage.

4. Results

This study will demonstrate how the repositioning occurred and how it increased favorability for RI. Results are presented chronologically within a framework centered on the time of repositioning (1200 UTC 27 August) focusing on four specific periods that document Dorian's transition from a misaligned vortex to an aligned vortex that undergoes RI:

1) Shear-driven vortex misalignment and dry air entrainment;
2) Tilt driven precipitation and vortex evolution within an environment of decreasing vertical wind shear;

[3] RMW is calculated using azimuthally averaged radial velocity. It is important to note that in reality the RMW has significant azimuthal variability during early-stage TCs like Dorian. And although vortex asymmetries can project differently onto the radial velocity, because the vortex moves from southeast to northwest over the radar site, the angle of the circulation center relative to the radar only significantly deviates for a short time period when the center is near the radar. More case studies are needed to quantify the reliability of these RMW (and center) estimates.

TABLE 1. List of properties and scanning strategies from the three ground radar sites used in this study.

Ground radar site	Martinique	Guadeloupe	Puerto Rico (TJUA)
Operationg Agency	Météo-France	Météo-France	NOAA
Wavelenth (cm)	10	10	10.7
Location	14.5°N, 61.02°W	16.31°N, 61.35°W	18.12°N, 66.08°W
Elevation (m)	380	30	902
No. of elevation angles	10	5	19
Scanning strategy	0°–10.5°	0.8°–4.2°	0.5°–19.5°
Sampling rate (min)	15	15	~5
Resolution	0.5° × 1 km	0.5° × 1 km	0.5° × 0.25 km
Maximum range (km)	256	256	460

3) Vortex repositioning and interactions with St. Lucia and Martinique;
4) Post-repositioning circulation development.

a. Shear-driven vortex misalignment and dry air entrainment (>9 h prior to repositioning)

Favorable environmental conditions for TC intensification generally require sufficiently warm sea surface temperatures (SST), low vertical wind shear, and a relatively moist troposphere (DeMaria and Kaplan 1994; Hendricks et al. 2010). Ocean heat content from 40 to 60 KJ cm^{-2} and 28°–29°C SSTs provided favorable oceanic conditions throughout Dorian's life cycle. Therefore, this section focuses primarily on determining the impacts from the vertical wind shear and dry air surrounding the TC core on vortex misalignment during the period more than 9 h prior to repositioning.

The vertical wind shear, defined here as the deep-layer shear from 850 to 200 hPa and radially averaged from 0 to 500 km of the TC center, is calculated using the ECMWF Reanalysis Version 5 (ERA5; Hersbach et al. 2020). Dorian remains embedded within an environment characterized by low deep layer shear (<10 kt) from 26 to 29 August. Despite this observation, Dorian initially has a displaced vortex structure, discussed in more detail below.

1) VORTEX MISALIGNMENT

The horizontal wind from TDR merged analyses (methodologies discussed in section 3) is plotted at four different vertical levels for the first P-3 flight, 12 h before repositioning (0000 UTC 27 August). Figure 3a reveals that the 2-km LLC has an RMW less than 50 km. The 4-km center (Fig. 3b) is displaced ~40 km to the northeast and has a much broader circulation with an ~70-km RMW. With increasing height, the center not only rotates anticyclonically but also extends farther radially outward from the LLC. Although the storm-relative wind speed at each level exhibits a pronounced asymmetry, a tilted[4] vortex core (defined by the RMW) is still identified, which exhibits substantial overlap in the 2–8-km layer.

2) VERTICAL WIND SHEAR

This tilted structure suggests that sub layers of shear, undetected by the commonly used deep-layer shear metric, are present that impacted the structure and evolution of Dorian. Therefore, following several recent studies of TC intensification in moderate shear (Finocchio et al. 2016; Ryglicki et al. 2019; Alvey et al. 2020) we examine the shear's horizontal and vertical distributions in more detail (Fig. 4).

To characterize the external environment, hodographs using ERA5 show the vertical wind profile within 150–500 km (Figs. 4a–d) of the TC center determined from the best track. The hodograph in Fig. 4a from 24 h before repositioning (1200 UTC 26 August) shows that despite low 850–200-hPa shear around 5 kt, layers of greater midtropospheric shear are apparent between 700 and 500 hPa (7.5 kt), 500 and 350 hPa (6.3 kt), and 350 and 200 hPa (11.1 kt) as the wind rotates anticyclonically with height. The shear directional change with height correlates strongly with the vortex structure shown in Fig. 3, a result also found in an idealized modeling study by Onderlinde and Nolan (2014). In response to weakening 850- and 700-hPa synoptic flow, the 850–700-hPa shear decreases to 0.2 kt and the 700–500-hPa shear decreases to 4.7 kt (Fig. 4b) 12 h before repositioning. Despite the low- to midtroposphere vertical wind shear weakening during this period, the continued vortex misalignment shown in Fig. 3 indicates a time-lagged response to the changing environment, a similar result to Onderlinde and Nolan's (2017) idealized modeling study.

The impact of vertical wind shear on the inner core can also be dictated by the horizontal distribution of vertical shear (Bukunt and Barnes 2015). A vortex removed shear is calculated by first identifying the vortex outer boundary, defined by the location outside of the RMW at which either the azimuthal mean tangential wind decreases below 5 kt or the azimuthal coverage of cyclonic tangential wind decreases below 75%. The vortex removal methodology then subtracts the wavenumber 0 component of radial and tangential wind within the determined vortex boundary at each vertical level. Focusing on the misalignment of the 2- and 6-km centers (Figs. 3a,c), Fig. 4e shows the vortex removed shear from 700 to 500 hPa, the layer also identified from Figs. 4a–d with the most significant decrease in vertical wind shear. Moderate values

[4] The usage of tilt and downtilt (or uptilt) throughout the manuscript is not meant to imply that the vortex is a singular, coherent tilted structure throughout the troposphere, but rather it is used for brevity following previous literature. It is possible that the vortices are not vertically continuous, and misaligned is more appropriate terminology.

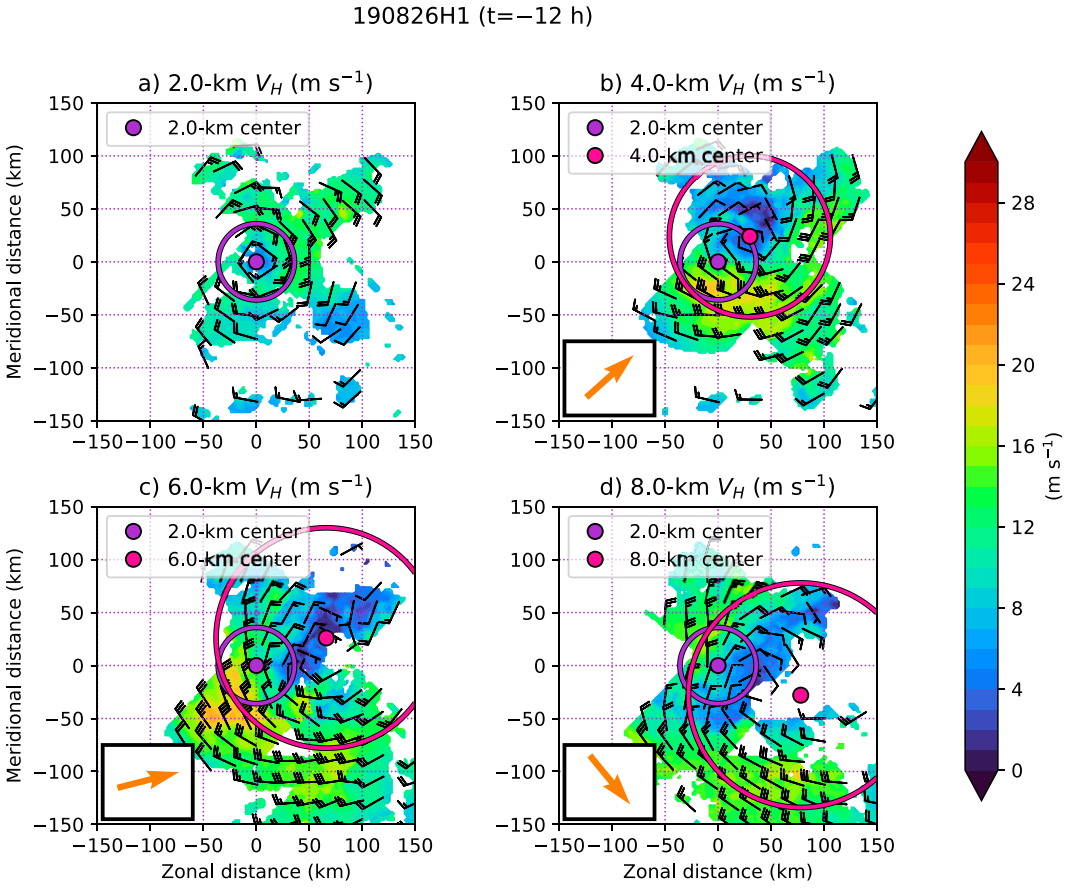

FIG. 3. (a) Storm-centered, storm-relative, horizontal wind at a height of 2 km observed by the TDR during the 190826H1 mission, approximately 12 h prior to the center reformation event. Wind speed (m s^{-1}) is shaded, with gray wind barbs showing the wind direction (kt). The length of the vector is proportional to the wind speed. The purple color-filled circle depicts the 2-km TC center location, while the purple unfilled circle denotes the 2-km RMW. (b)–(d) As in (a), but for heights of 4, 6, and 8 km, respectively, with the magenta dashed circle denoting the RMW at those heights. In each panel, the axes of the domain are relative to the 2-km TC center location and the magenta dot depicts the height-relative TC center estimate. The orange arrows in the lower left boxes of (b)–(d) indicate the ERA5 calculated 0–500-km shear vector in the 2–4-, 2–6-, and 2–8-km layers, respectively.

(15–20 kt) of west-southwesterly vertical wind shear within this midtropospheric layer (700–500 hPa) are clearly shown impinging upon the inner core around 1200 UTC 26 August (−24 h), further supporting the misalignment magnitudes evident in Fig. 3.

3) RELATIVE HUMIDITY

Because Dorian remained embedded within a relatively dry environment throughout its early life cycle, this subsection links the asymmetric distribution of humidity to the vertical wind shear and provides an overview of the impact of dry air on the inner core. The midtropospheric relative humidity (RH, 700–500 hPa) calculated from ERA5[5] output ranges from only 35%–40% within a 200–800-km annulus[6] (not shown) during the time periods surrounding repositioning (26–27 August). The NHC tropical cyclone report cited this dry air as a possible inhibitor of intensification (Avila et al. 2020). The biggest question, however, is whether dry air reached Dorian's inner core and suppressed convection, either by lateral mixing into eyewall updrafts (Tang and Emanuel 2010, 2012), or by enhancing the boundary layer flushing response to shear and thereby stabilizing the boundary layer (Riemer et al. 2010).

Figure 5a shows the radial distribution of the 700–500-hPa RH calculated from ERA5 on 26–29 August. In the 12–36-h window preceding repositioning (0000 UTC 26 August–0000 UTC 27 August), an apparent intrusion of dry air well within the inner core decreases the 0–100-km RH from 80% to 65%. Very dry air 300–600 km from the center is also

[5] The ERA RH fields compare favorably with G-IV dropsondes (not shown), and the ERA TC center is within 30 km of the TDR center locations.

[6] Similar to the SHIPS parameter, SHRD.

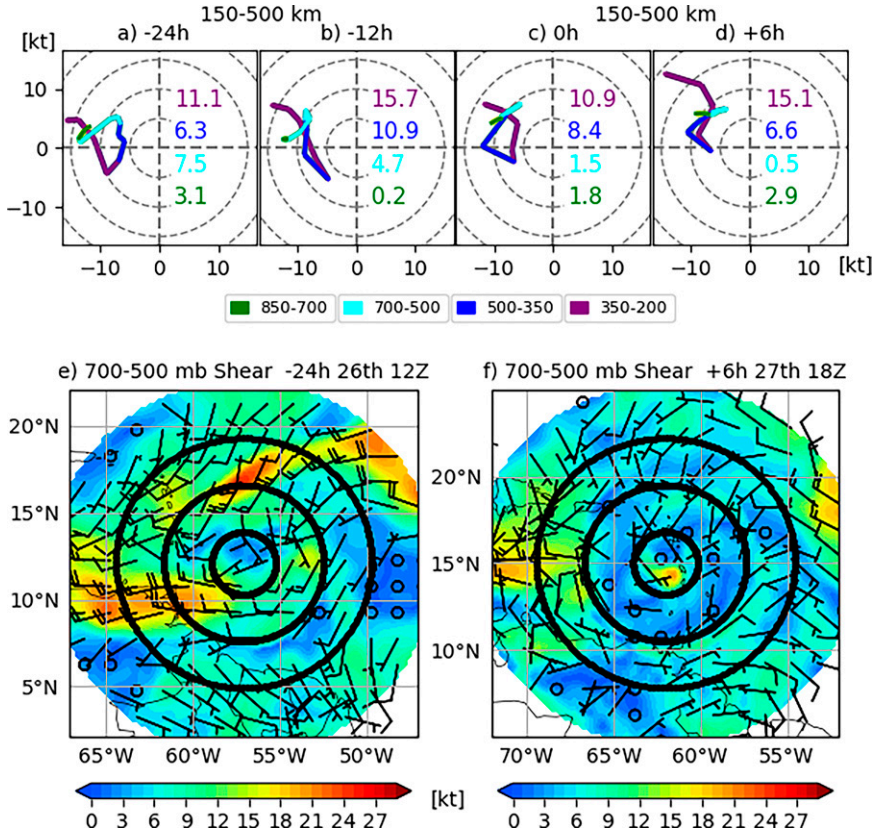

FIG. 4. Hodographs derived from ERA5 at (a) 1200 UTC 26 Aug, (b) 0000 UTC 27 Aug, (c) 1200 UTC 27 Aug, and (d) 1800 UTC 27 Aug calculated within 150–500 km of the center. Different color lines denote the vertical layers: 850–700 hPa (green), 700–500 hPa (cyan), 500–350 hPa (blue), and 350–200 hPa (purple). Each dashed radial ring represents 5 kt. The numbers in (a)–(d) indicate the calculated shear magnitudes for each time with the color corresponding to its aforementioned shear layer. Horizontal plan views of ERA vortex-removed shear at (e) 1200 UTC 26 Aug and (f) 1800 UTC 27 Aug. The black circles are the 200-, 500-, and 800-km radii.

observed, which is the likely source for reduced inner core values.

Given the vortex's misaligned structure in Fig. 3, it is unsurprising that this period also featured dry air entrainment. Nonetheless, better understanding why dry air entrained into the inner core on 26 August (12–36 h before repositioning) is necessary, particularly for periods without detailed vortex structure information provided by aircraft. Figures 5b and 5c presents a new diagnostic that shows the potential synergy between the magnitude and azimuthal location of vertical wind shear and RH by including the quadrant-based spatial distribution in the 700–500-hPa layer, where shear is hypothesized to be the most detrimental, and from 0 to 300 km from the storm center. This radial distance is chosen to encompass the inner core and near inner core environment. The radial length of each azimuthal bin corresponds to the mean vertical wind shear within that azimuth, whereas the color fill corresponds to the relative humidity. For the period 24 h before repositioning (1200 UTC 26 August, Fig. 5b), the northeast–-north-northwest quadrants (downshear of the 700–500-hPa vector) have a humid midtroposphere (>80%) and relatively low values of vertical wind shear, less than 5–10 kt. On the other hand, much drier midtropospheric air (<50%) is apparent on the southern side of the storm (upshear of the 700–500-hPa vector), also coincident with the largest shear values (15 kt, southwest quadrant). This configuration likely initially allowed dry air entrainment into inner core precipitation and limited the overall precipitation symmetry, described in more detail in section 4b. The dry midtropospheric air upshear (700–500-hPa shear vector) is in a location where it can be advected above the LLC in the midlevels, unfavorably inhibiting convection through entrainment or a capping inversion near the LLC.

To more explicitly show lateral entrainment of dry air, Fig. 6 illustrates the 5-km flow from the TDR merged analyses on 0300 UTC 27 August (−9 h, Fig. 6a) and 0000 UTC 28 August (+12 h, Fig. 6c) following similar methodologies from Willoughby et al. (1984) and Riemer and Montgomery (2011). The RH (color contours) is from ERA5 at corresponding times and vertical levels. At 0300 UTC 27 August (−9 h) both the 5- and 2-km centers are located within ~70% humidity; however, RH values rapidly decrease to less than

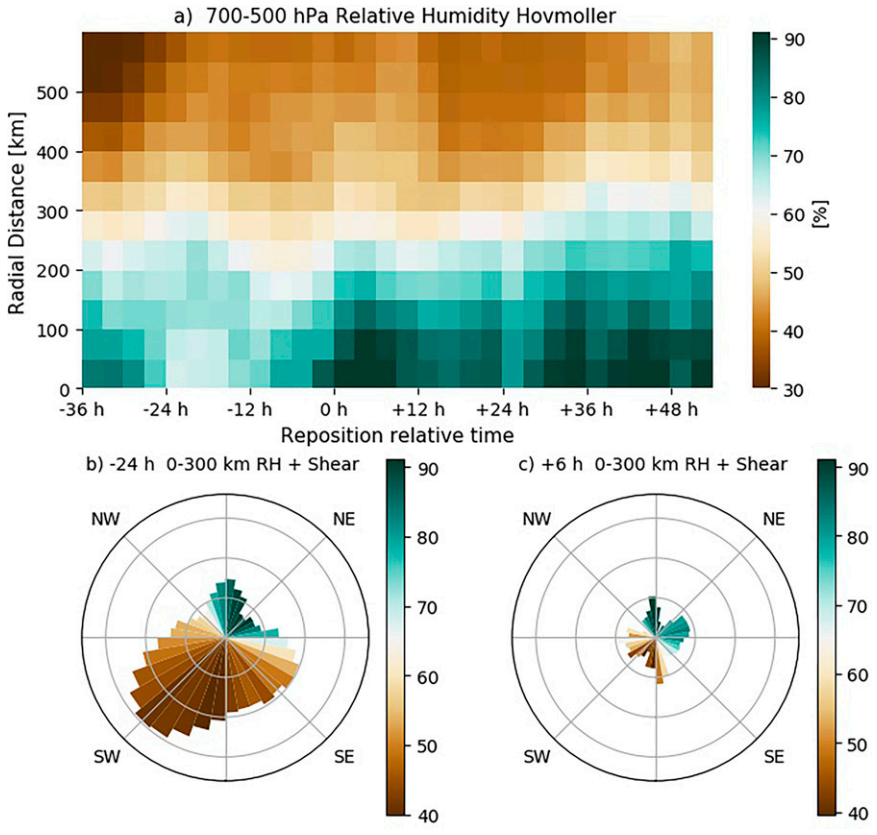

FIG. 5. (a) The ERA 700–500-hPa RH Hovmöller averaged within different radii of the center (y axis). (b),(c) Midtropospheric RH (700–500 hPa) averaged within 0–300 km (color shading) for 10° azimuthal bins with respect to the center for −24 h [1200 UTC 26 Aug in (b)] and +6 h [1800 UTC 27 Aug in (c)]. The radial bin length represents the 0–300-km vortex removed 700–500-hPa shear magnitude in each azimuthal bin, and each radial ring represents 5 kt.

50% only ~50 km toward the south, near the LLC's RMW. Although the flow vectors are relatively parallel to the RH contours by this time period, the proximity of radial inflow (not shown) of dry air to the center indicates that some dry air was previously advected into the inner core. This is likely linked to the dry air intrusion mentioned above around 1200 UTC 26 August. This RH configuration limited precipitation in Dorian's southern quadrant and contributed toward the asymmetric precipitation distribution shown in section 5b. In summary, the combination of dry midtropospheric air, vertical wind shear, and previously induced misalignment likely precluded intensification during this pre-repositioning period.

b. *Tilt-driven precipitation and vortex structure in decreasing vertical wind shear (9–3 h prior to repositioning)*

Although the vortex structure is observed using TDR wind analyses from the P-3 flights on 26–28 August (Figs. 1a,c), as illustrated in Fig. 3, the once-a-day flights only provide snapshot views before and after repositioning. Because Dorian undergoes significant structural evolution with vortex repositioning around 1200 UTC 27 August (i.e., 12 h between the daily P-3 flights shown in Fig. 1c), center tracks for the low-level (0–2 km) and midlevel (4–6 km) vortex are determined using CAPPIs of the radial velocity from Martinique and Guadeloupe ground radars. Figure 7 demonstrates the vortex evolution by displaying these "parent" vortex tracks (described with more detail in the methodologies, section 3) and their approximate RMW at different vertical levels prior to, during, and following the period in which Dorian underwent a center repositioning. It also includes TDR-derived center estimates for comparison.

At 0400 UTC 27 August, 8 h before vortex repositioning, Fig. 7 shows that the center of the MLC remains displaced to the northeast of the near-surface vortex center by ~50 km. This agrees reasonably well with the more detailed TDR wind analyses (Fig. 3) from just a couple of hours earlier, outlined by the black and red circles. From −8 to −4 h before repositioning (0400–0800 UTC) the low- and midlevel vortices remain displaced despite decreasing vertical wind shear below 500 hPa (Fig. 4b). After 0800 UTC (−4 h), the surface circulation broadens, evidenced by the expansion in 2-km RMW (Fig. 7). The importance of this observation will be expanded upon in section 4c.

Delineating the precipitation type, as shown in Fig. 8, is important considering that different precipitation types have

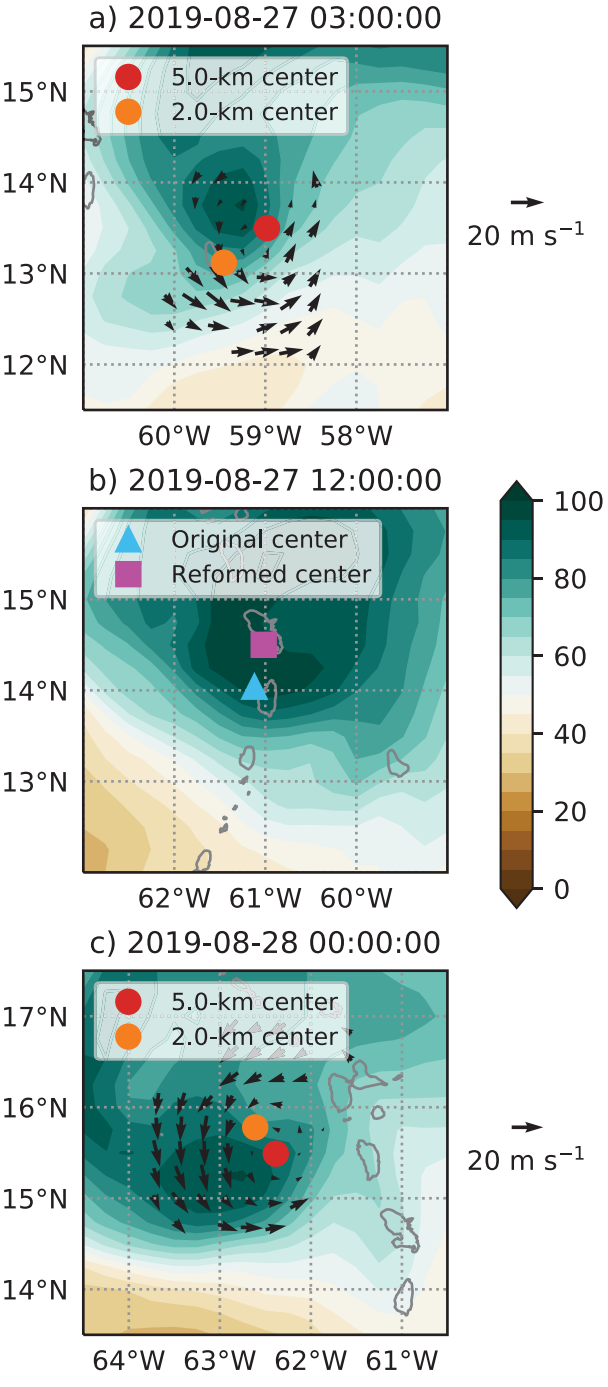

FIG. 6. The 700–500-hPa layer-mean RH (shaded; %) from ERA5 analyses at (a) 0300 UTC 27 Aug (−9 h), (b) 1200 UTC 27 Aug (0 h), and (c) 0000 UTC 28 Aug (+12 h). Storm-relative winds at a height of 5 km are shown by the black vectors, derived from TDR observations from the 190826H1 mission in (a) and the 190827H1 mission in (c). When TDR observations are available, the TC center positions at heights of 2 and 5 km are shown by the orange and red markers, respectively. The original (blue) and reformed (pink) center identified by ground radar at the time of the RH analysis are shown in (b).

distinct latent heating and mass flux profiles that can uniquely influence thermodynamic profiles and vortex structure of early-stage TC formation (Raymond and Sessions 2007; Rogers et al. 2020; Rios-Berrios 2020). Dorian's initially compact inner core has most precipitation located within 1° of the LLC 6 h before repositioning (0600 UTC 27 August, Fig. 8a). Most of the moderate and deep convection are concentrated in the downtilt (northern) quadrant, an expected precipitation distribution given the misalignment. Although the uptilt quadrant generally has less precipitation than found downtilt, the somewhat symmetrical distribution of stratiform precipitation within 30–40 km of the LLC, particularly uptilt, is considered a favorable configuration for future intensification (Alvey et al. 2020). The partitioning algorithm also identifies anvil cloud located 0.5°–1° from the center in the western quadrant (left of tilt). This may indicate that locally driven outflow from persistent downtilt deep convection is resisting any upper-tropospheric vertical wind shear shown in Figs. 4a and 4b, a hypothesis explored by Ryglicki et al. (2019) and Alvey et al. (2020).

As seen in the 0.6° elevation scans of reflectivity and 1-km CAPPI velocity from Martinique's ground radar between 5.5 and 3.5 h pre-reposition (0630–0830 UTC; Figs. 9a,c,e) the inner core structure appears to degrade, nearly coincident with the LLC broadening described above (Fig. 7). The strongest near-center convection weakens from >50 to 35–45 dBZ and forms into a lobe or banded structure near the RMW that extends anticyclonically outward southwest–northeast from the surface center.

To further quantify the spatial and temporal evolution of different precipitation types, Fig. 10 shows the percent areal coverage within 200 km (Figs. 10a–c) of Dorian's center and within the 0–2-km RMW (Figs. 10d–f). Although this pre-reposition period (from −8 to −2 h) initially features some of the lowest coverages of stratiform (15% within 200 km, 25%–50% within RMW × 2), it gradually increases within 6 h of repositioning. A convective burst (CB) is observed that peaks around 5 h prior to repositioning but is shortly followed by a convective minimum that importantly coincides with the broadening LLC and outward-propagating convective band described above.

In summary, this pre-repositioning period is characterized by a misaligned vortex and broadening LLC, commonly associated with weakening TCs. However, the next section will provide details that show the LLC's broadening just prior to the repositioning period likely enabled more effective maximization of confluence near convection and diminished negative effects from misalignment that include weaker enthalpy fluxes (Schecter and Menelaou 2020).

c. Vortex repositioning and interactions with Martinique and St. Lucia (from 3 h prior to 3 h after repositioning)

The sequence of events during this critical period includes the following:

1) Continued decrease in convection near the weakening LLC;

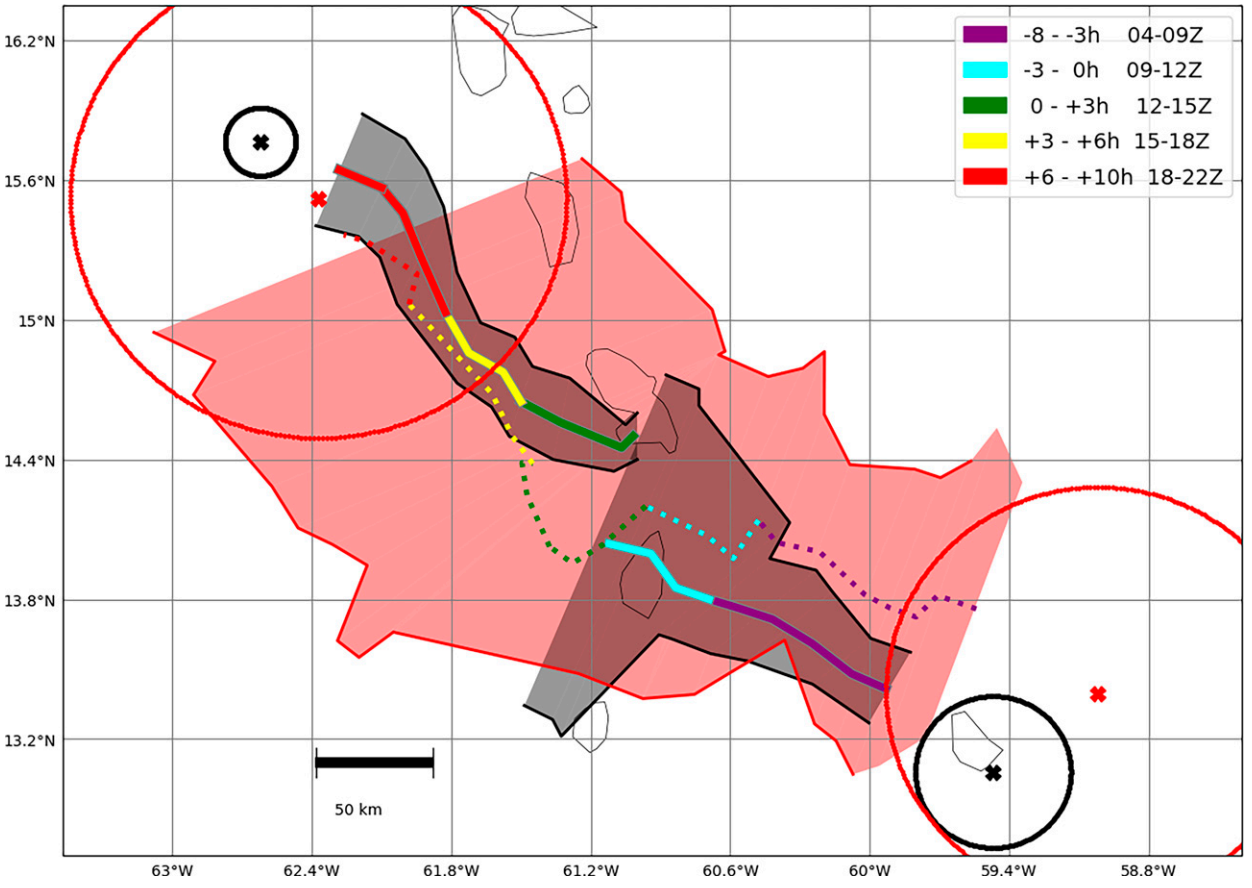

FIG. 7. The 27 Aug 0–2-km (solid line) and 4–6-km (dotted line) center tracks determined using Martinique and Guadeloupe ground radar radial velocities with their color corresponding to the time of each center's location and its hour relative to reformation. The gray shading indicates all of the area inside of the 0–2-km RMW. The red shading indicates all of the area inside of the 4–6-km RMW. The black and red X marks (circles) indicate the 0–2- and 4–6-km center locations (RMWs), respectively, determined from TDR analyses from two P-3 flights (190826H1, 190827H1).

2) Subsequent increase in deep convection that persists for several hours near Martinique;
3) A distinct relocation of the LLC to the northeast of the MLC into a more humid environment near 1200 UTC 27 August.

The coverage of deep convection within the RMW (and ~75 km from the center) continues to rapidly decrease (Fig. 10f) from 3% to less than 1% at −2.5 h (Fig. 9g, 0930 UTC). This lack of convection near the original LLC likely contributed to a reduction of inflow, spin down, and a broadening of the wind field (Fig. 7). Although St. Lucia likely played a role in weakening the LLC due to land interaction, other processes may have also contributed to the structural transformation given the observed broadening and convective decrease prior to land interaction.

During this same period, the overall precipitation expands farther radially outward (Fig. 8b, −2 h) with large increases in the coverage of convection 75–200 km from the LLC, particularly downtilt. Around 30 min before repositioning (1130 UTC 27 August), upon the parent LLC's emergence into the Caribbean Sea from St. Lucia, an Air Force reconnaissance mission transects the circulation from southwest to northeast. Figure 11b shows the radar reflectivity from Martinique's ground radar with the reconnaissance flight level winds (1.5-km altitude) and extrapolated surface pressure overlaid. The reconnaissance winds indicate a much broader circulation than the previous reconnaissance passes, 7 h prior (Fig. 11a). The black circle highlights the ground radar deduced RMW at ~80 km (Fig. 11b), a magnitude that appears to align reasonably well with the flight-level wind RMW. The aircraft extrapolated surface pressure in Fig. 11d (cyan color) also indicates that the LLC weakened, evident by the minimum sea level pressure rising 3 hPa from the previous pass at −7.5 h (purple color).

Approximately one hour before repositioning, deep convection increases downtilt, but well beyond the MLC center, near the southern end of Martinique (Fig. 9i). By 1130 UTC, (−0.5 h; Figs. 8c, 10c, and 11b), a CB intensifies over Martinique, coincident with a convergence line[7] interacting

[7] This feature represents a band-like structure with low-level convergence observed in the radial velocity.

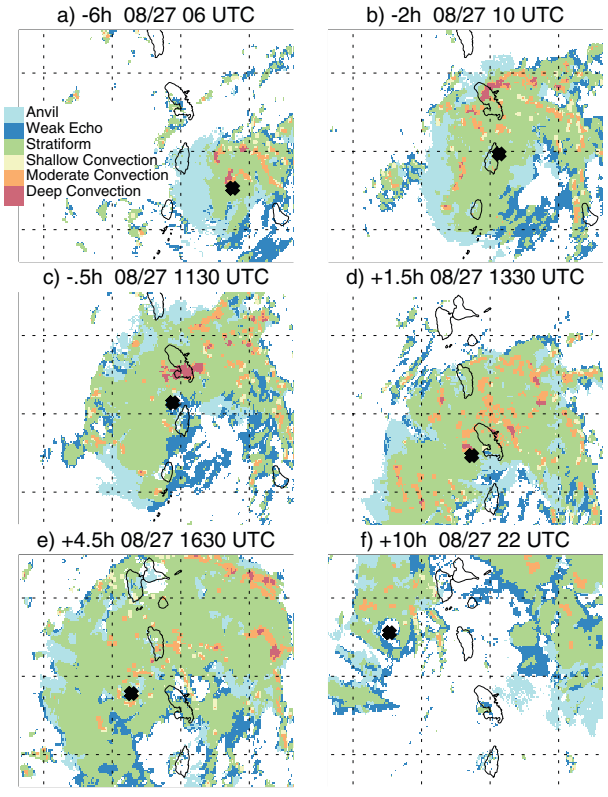

FIG. 8. Precipitation partitioning using Guadeloupe and Martinique (Météo-France) radars. The dashed grid is spaced every 1° of latitude and longitude. Precipitation types are delineated by color pixels in the figure as follows: anvil (light blue), weak echo (dark blue), stratiform (green), shallow convection (yellow), moderate convection (orange), and deep convection (red). Partitioning was done using a combination of radars and extrapolated to CAPPIS. The X denotes the radar designated center for each time.

with the island (Figs. 9h,j,l; dotted line) along the northern portion of the preexisting, broadening LLC, and northward RMW expansion. Quantified in Fig. 10c, this deep CB exhibits one of the largest, most concentrated convective developments during Dorian's early life cycle and we believe is a critical factor in Dorian's LLC repositioning. A persistent mesovortex-like feature develops (Figs. 9k,l,m,n) and eventually consolidates into the new low-level vortex that continues to organize through 1400 UTC (Figs. 9o,p), 2 h after repositioning. Circulation formation from particularly intense CBs has also been seen in some previous observational studies during TC genesis (Reasor et al. 2005; Houze et al. 2009; Bell and Montgomery 2010). Although Dorian's vortex repositioning is consistent with the reformation paradigm, it is also possible that convergent flow from the downtilt CB induced positive horizontal vorticity advection further contributing to spin up. Furthermore, the environmental background of this vortex repositioning differs from past literature documenting reformation (Nguyen and Molinari 2015; Chen et al. 2018; Rogers et al. 2020), wherein the vertical wind shear is greater than the low magnitudes in Dorian (Figs. 4b,c). In addition, the new LLC forms northeast beyond the center of the MLC, whereas many of the aforementioned studies observed reformation beneath the center of the MLC. While the displacement between the LLC and MLC immediately after reformation appears larger than before (Fig. 7), some of this may have been due to uncertainties in the center-finding algorithm near the radar. By 3 h, though, the displacement reduced, suggesting that this reformation may have played a role in alignment.

What is also unique with this case is that island interaction appeared to invigorate the deep CB that formed into the repositioned LLC. Figure 12 examines Martinique's potential enhancement of the CB in more detail by showing the temporal evolution of an along-flow (east-southeast–west-northwest) reflectivity cross-section as the convergent line (Fig. 9j) approaches the island from the ESE. Even before reaching Martinique, (10–20 km from the coast) reflectivity increases as shallow convection (20-dBZ echo top, 3–5 km) develops into moderate–deep convection (20-dBZ echo top, 8 km). Upon reaching Martinique, the CB continues to intensify with >40-dBZ echoes dominating the low- to midtroposphere (0–5 km), and 30-dBZ echoes extending up to 10 km. As the CB peaks near 1130–1145 UTC, while traversing southern Martinique's highest topography (~400 m), multiple mesocyclonic signatures develop in the radar reflectivity, indicated by "hook echoes" (Figs. 12d,e, bottom panels). Several studies have shown terrain deflection or dynamically driven lee-cyclone reformation in previous TCs with larger vertical and horizontal terrain obstacles (Bender et al. 1987; Lin et al. 2002); however, it is unlikely this played a dominant role given that the reformed vortex emerges along the southwest tip of Martinique (Figs. 9k–p), wherein topography peaks near only 400 m (Fig. 12). Rather, given the location of the emergence of a low-level mesocyclone associated with the CB downtilt, the authors speculate that the greater surface roughness (friction) in this easterly flow regime played a more dominant role in mechanically driven convective invigoration, a phenomenon observed by Wang and Sobel (2017) in a study investigating the effects of high wind on rainfall surrounding small tropical islands. To more definitively determine whether Martinique played a role in the evolution of the CB, the authors acknowledge that high-resolution simulations would be required with artificial topography and land removal, which is beyond the scope of this study.

An important question that has not yet been fully addressed: What other vortex scale and environmental characteristics allowed the deep convective burst and repositioning to occur? The previously mentioned broadening of the LLC likely provided a more effective background for increasing confluence associated with the reformative convective burst. By the time of repositioning (0 h, Fig. 4c) the vertical wind shear in all layers has decreased to 10 kt or less. Figure 6b shows the center positions of the remnant LLC after crossing St. Lucia (blue triangle) and reformed LLC near Martinique (pink square) with respect to the midlevel RH. Between this time period and 9 h earlier (Fig. 6a), the RH maximum increases from ~90% to greater than 95% and expands radially outwards in the northern quadrants by

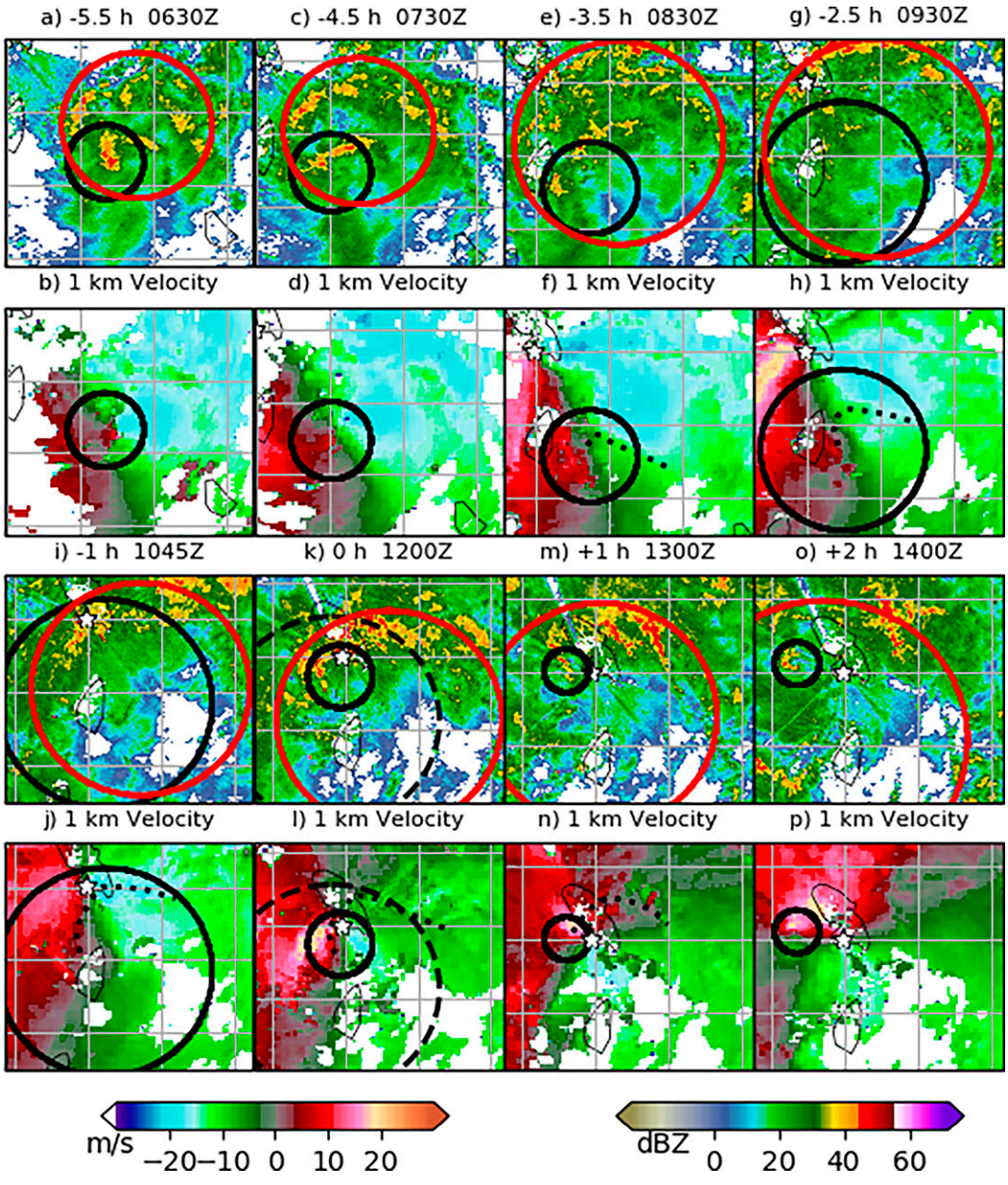

FIG. 9. (a),(c),(e),(g),(i),(k),(m),(o) Martinique's ground radar (white star) with the 0.6° elevation angle reflectivity (dBZ) and (b),(d),(f),(h),(j),(l),(n),(p) 1-km Doppler velocity (m s^{-1}) from the interpolated CAPPIs. Each gray grid line represents 0.5° of longitude or latitude. The black circle indicates the coarse-filtered 0–2-km RMW determined from ground radar and red circle marks the 4–6-km RMW. The dashed circles in (k) and (l) represent the old, remnant LLC. The dotted lines in (f), (h), (j), (l), and (n) denote a subjectively identified outwardly propagating convergence line.

100–200 km. Perhaps most importantly, Fig. 6b also shows that the vortex reforms farther within the more favorable high midtropospheric RH region.

During this repositioning period, stratiform precipitation also plays an important role. Stratiform's previously symmetric (Fig. 8b) coverage dissipates near St. Lucia (Fig. 8c), perhaps due to vortex spin down and proximity to environmental dry midtropospheric air shown in Fig. 6b. Figure 10a also reveals that stratiform precipitation within 200 km markedly increases from 15% to greater than 40% from −6 to +3 h (0600–1500 UTC 27 August). Interestingly, stratiform's increase begins nearly coincidentally with the development of deep convection (Fig. 10c). The stratiform coverage, however, continues to increase even after the deep convection peaks near 1200 UTC, likely a reflection of the maturation of precipitation processes and similar to the evolution first noted by Houze (2004) in mesoscale convective systems and

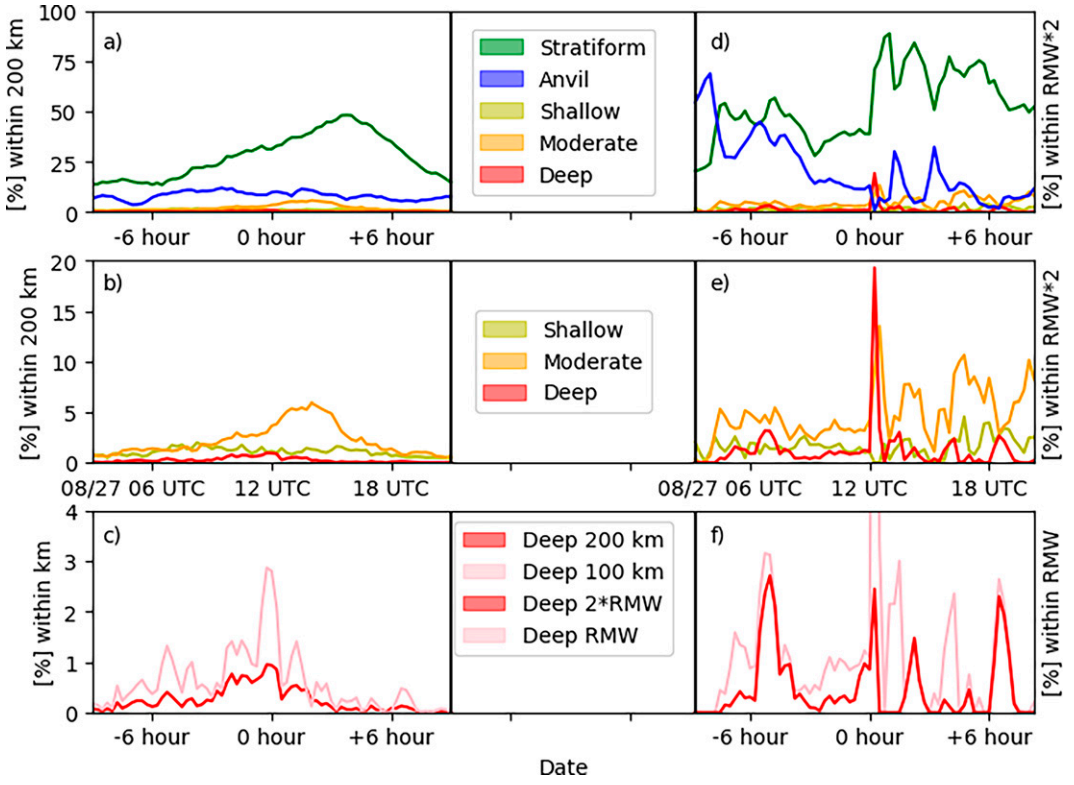

FIG. 10. Percent areal coverage for partitions of anvil (blue), stratiform (green), shallow convection (yellow), moderate convection (orange), and deep convection (red) within 200 km (a),(b) from Météo-France's Martinique and Guadeloupe ground radars. (c) Deep convection calculated within 100 km (pink) and 200 km (red) is delineated. (d)–(f) As in (a)–(c), but percentages are calculated within 2 RMW in (d) and (e) or 1 RMW in (f).

later applied to TCs (Houze 2010; Didlake and Houze 2013). The expansive and robust stratiform region throughout this period may have also contributed to the MLC's maintenance (Houze 2004) despite its displacement from the LLC. At 1330 UTC (+1.5 h, Fig. 8d), stratiform precipitation again symmetrically covers all quadrants within the inner core. This stratiform precipitation, although it initially stabilizes (Zawislak et al. 2016) the boundary layer, can also favorably moisten the low- to midtroposphere and precondition the environment for more sustained convection (Alvey et al. 2020) following renewed favorable boundary layer thermodynamics. Overall, a similar evolution was noted in Hermine (2016; Rogers et al. 2020), where the development of a persistent aligned circulation occurred in the presence of deep and moderate convection that developed where the local environment was moistened and stabilized by persistent precipitation downshear of the long-lived LLC.

d. Post-repositioning circulation development (>3 h after repositioning)

The compactness of the new low-level vortex (~30-km diameter) likely contributed to more rapid spin up (Chen et al. 2011; Carrasco et al. 2014) as it moved toward the northwest. Reconnaissance verifies the development of the new, small circulation center and lower pressure minimum by +4 h (Fig. 11c, 1615 UTC). Azimuthal shear from the ground-based Doppler velocity is used as a proxy for the vortex's rotational strength by taking the difference between the average inbound and outbound velocities within 1.5 RMW, similar to mesocyclone and tornado vortex algorithms (Mitchell et al. 1998). Although the rotational velocity of the repositioned vortex (Fig. 13, delineated by values greater than 10 m s^{-1}) initially only extends upward to 2–3 km through 1600 UTC (+4 h), nonnegligible rotational velocity (generally 10 m s^{-1} or less) is also observed in the mid- to upper troposphere (5–10 km). This likely at least partially reflects either the preexisting broad MLC or a transient mesocyclonic circulation from the reformative CB that extends into the mid- to upper troposphere. From 1700 to 1930 UTC (from +5 to +7.5 h) the 4–8-km rotational velocity[8] significantly increases from 7.5 to 12–15 m s^{-1}, an indication of the vortex deepening.

Throughout this period of increased organization and reintensification, the preexisting broad MLC persists to the south and southeast of the reformed low-level vortex, displaced by 25–50 km (cf. Fig. 7). Despite the structure persisting in this configuration with the center of the preexisting MLC displaced from the reformed LLC, the more humid environment

[8] Symmetric precipitation during this period affords a large areal coverage of near-center velocity data necessary for rotational velocity calculations.

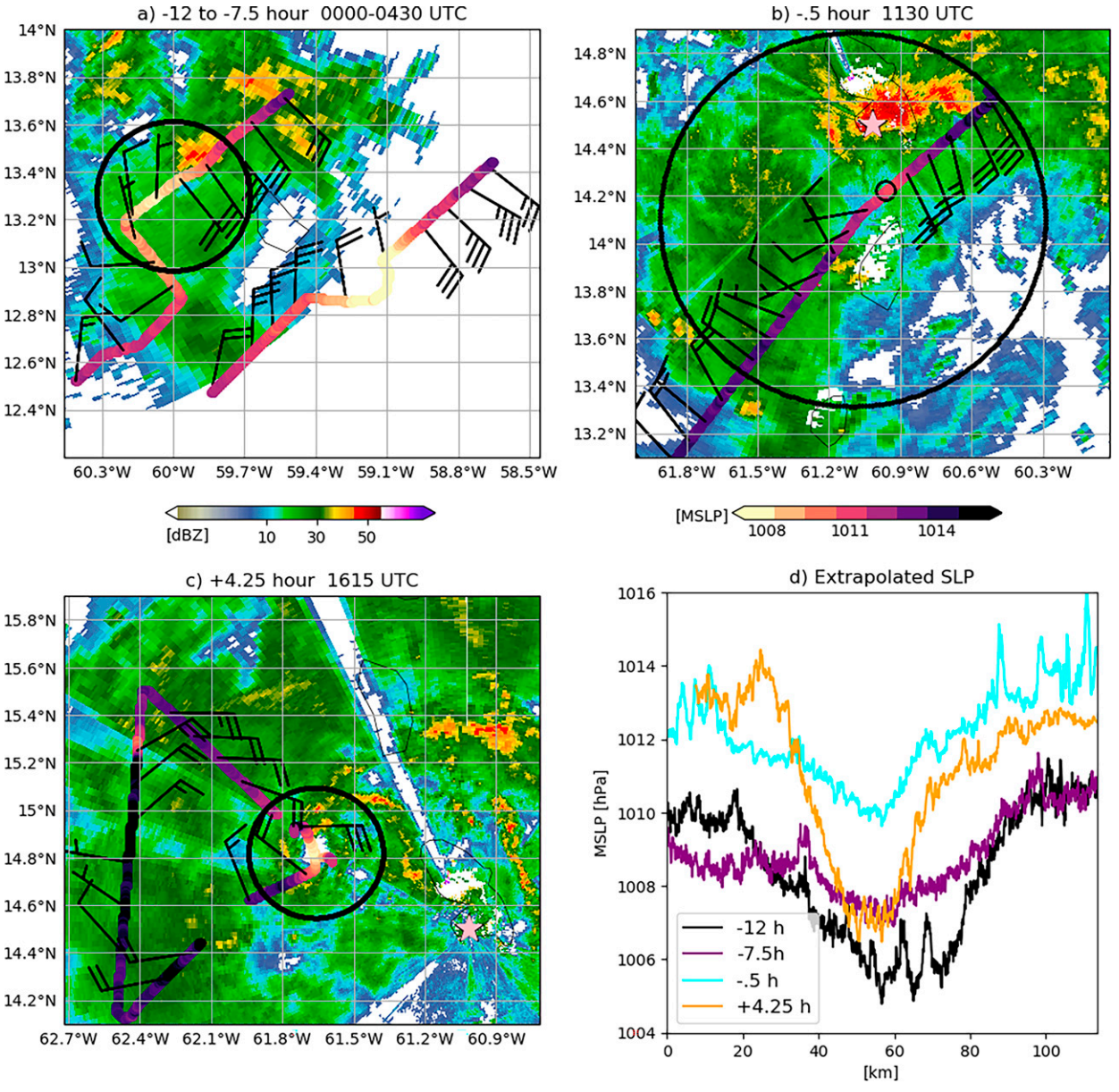

FIG. 11. (a)–(c) Martinique's ground radar with the 0.6° elevation angle reflectivity (dBZ). The black circle indicates the radar determined 0–2-km RMW. The Air Force Reconnaissance ~1.5-km flight-level winds are plotted with black wind barbs. The color coding along the line indicates the aircraft's extrapolated surface pressure. The pink star indicates Martinique's radar location in (b) and (c). (d) The extrapolated surface pressure for all flight tracks in (a)–(c).

within the MLC's broad structure (evidenced by the 4–6-km RMW greater than 70 km; Figs. 3b,c) still overlaps the LLC that gradually deepens (Fig. 13) through the +3 to +6 h following repositioning.

An important question remains partially unanswered: What changed from previous time periods that enabled the repositioned circulation to persist and intensify? Figure 8e shows a more symmetric distribution of moderate convection near the LLC (more orange color around the X mark on Fig. 8e) by 1630 UTC (+4.5 h). This is also consistent with Fig. 10e, which shows moderate convection peaking near 10% (within RMW × 2) 5 h after the deep convective burst and repositioning occurs. This concentration and/or increased frequency of moderate convection in pre-RI storms has been found in several passive microwave composite studies (Zagrodnik and Jiang 2014; Alvey et al. 2015), and is consistent with Rogers et al. (2020) who showed that this greater proportion of moderate convection may exhibit increased stability and a shift toward a more bottom-heavy mass flux profile that sustains convergence in the newly formed low-level vortex.

The persistence of this favorable moderate convection distribution was likely enabled by several factors. At +6 h

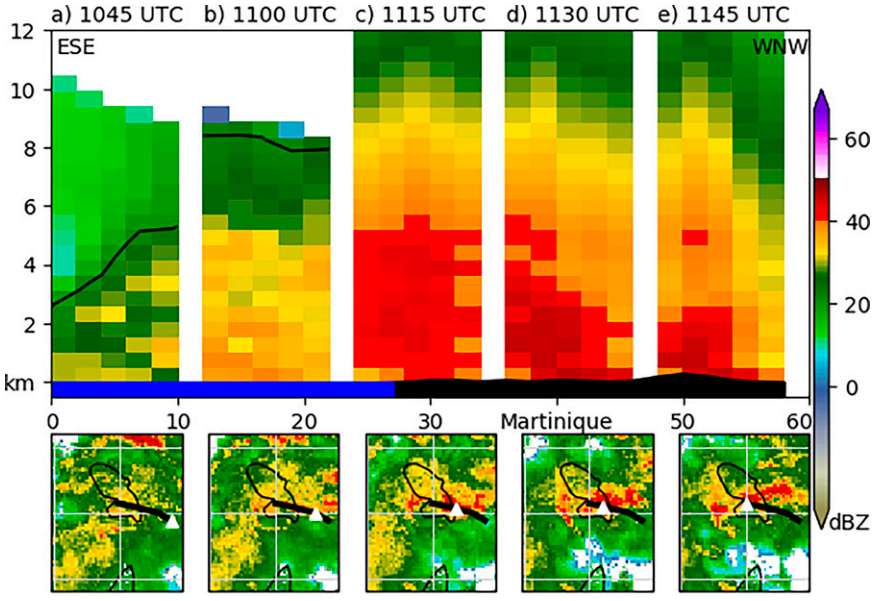

FIG. 12. Snapshots of along-flow (east-southeast–west-northwest) vertical reflectivity cross sections using CAPPIs of Martinique's and Guadeloupe's radars at (a) 1045, (b) 1100, (c) 1115, (d) 1130, and (e) 1145 UTC 27 Aug. (top) The black lines in the vertical cross sections indicate the 20-dBZ contour. Martinique's topography is indicated by the black shading (to scale) and Atlantic Ocean by the blue shading at the bottom of the vertical cross sections. (bottom) The corresponding plan views of 2-km reflectivity with the entire vertical cross section marked by a black line and white triangles denoting the start location of each time's east-southeast–west-northwest cross section.

(Fig. 4d, 1800 UTC 27 August), while the hodograph still shows a similar shear profile within the 350–200-hPa layer as 30 h prior, shear decreases throughout the 700–350-hPa layer. Near RI onset (+6 h, cf. Fig. 5c), although the RH is still quite dry (40%–50%) in the southwest quadrant, considerable humidification is observed in the southeast quadrant (Fig. 5c). Humidification near and within the inner core, also observed in Fig. 5a, is likely the result of three processes to varying degrees: 1) Vortex reformation toward the northeast, in preexisting higher humidity values (Figs. 6b,c); 2) Moistening and gradual humidification even prior to repositioning (Fig. 5a) caused by large increases in the areal coverage of precipitation, particularly moderate convection and stratiform (Figs. 8 and 10a); and 3) Reduction in midlevel shear in all quadrants (Figs. 4d,f and 5c).

By 10 h after repositioning, (Fig. 8f, 2200 UTC 27 August) all precipitation decreases in the southern semicircle, a similar distribution to the 0000–0200 UTC 28 August P-3 flight's TDR reflectivity coverage (not shown), possibly a reflection of stabilization following the vigorous stratiform episode in the previous 12 h. This may also be related to the temporal variability in relative humidity and precipitation associated with the diurnal cycle (Figs. 5a and 10) as this decrease in precipitation occurs during the expected diurnal minimum (Dunion et al. 2014).

Figures 14b–d reveals that the broad structure of the mid- to upper-level vortex observed during the P-3 flight +12 h after repositioning remained relatively unchanged from the flight 24 h earlier. The biggest change over this period is the structure and location of the newly reformed 0–2-km center (Fig. 14a), now located to the north of the broad MLC center, as observed earlier at the time of the repositioning. An analysis of TDR-derived vorticity (not shown) indicates vertical penetration of elevated positive values into the 4–6-km layer above the reformed low-level vortex. Thus, convective processes are active locally to modify the midtropospheric vorticity, but still insufficient at this time to produce a closed circulation within the broader preexisting midlevel cyclonic flow.

During the period between 190927H1 and 190928H1 (0000 UTC 28 August and 0000 UTC 29 August P-3 flights), the reformed vortex continued to develop and deepen despite its misalignment from the persistent, broad MLC, and began a period of rapid intensification. The 190928H1 P-3 flight overflew Dorian near 2300 UTC 28 August, near the end of the rapid intensification period. Figure 15's merged TDR analysis from this period reveals a much more robust, compact low-level vortex with winds at 2 km (Fig. 15a) now exceeding 30 m s^{-1}. Significant changes were also observed with the MLC (Figs. 15b–d), now more closely aligned with the 2-km vortex center (Fig. 15a) than seen during the previous flight 24 h earlier (Fig. 14). The 4- and 6-km winds (Figs. 15b,c) suggest the compact LLC observed approximately 24 h earlier had stretched vertically, with a much smaller RMW observed at this time, despite signs of the remnant broader RMW identified by a local maximum in wind speed at radii of approximately

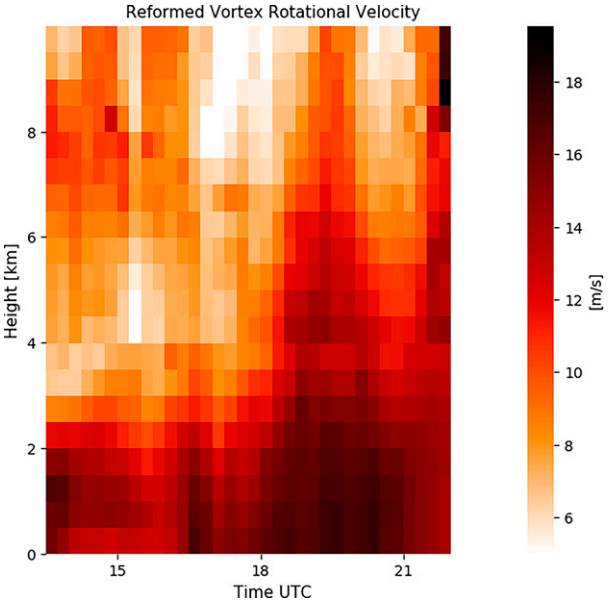

FIG. 13. A Hovmöller with respect to height of the reformed vortex's rotational velocity calculated from Martinique and Guadeloupe ground radars on 27 Aug.

50–75 km. This vertical development of the compact LLC upward into the midlevels agrees with TJUA radar observations (not shown).

5. Discussion

This study examines the complex kinematic and thermodynamic evolution of a weak tropical cyclone as it organizes into a more aligned circulation that undergoes rapid intensification. The temporal evolution of these fields is facilitated by a unique synthesis of multiplatform analyses. NOAA's P-3 (in situ and TDR) provides the foundational three-dimensional vortex structure, whereas multiple ground radars from Météo-France and complementing Air Force Reconnaissance in situ flight level data fill gaps during Dorian's vortex restructuring.

Dorian's early stage evolution begins with a misaligned vortex and relative humidity asymmetries induced by vertical wind shear (from −12 to −24 h prior to repositioning). Despite weakening vertical wind shear, the vortex remains misaligned with asymmetric precipitation and humidity prior to repositioning. As the primary LLC nears St. Lucia, it broadens and weakens, coincident with a decrease in near-center convection. A convergence line subsequently interacts with Martinique causing an increase in deep convection that forms into one of the most concentrated CBs of Dorian's early life cycle. The development of a mesocyclone from this convective burst ultimately forms a new, compact LLC within the broad cyclonic envelope that eventually deepens and rapidly intensifies despite some continued misalignment. The most important findings from this sequence of events are detailed as follows.

In spite of relatively weak deep-layer shear (e.g., 3–5 m s^{-1}), the MLC center of Dorian was initially displaced downshear from the LLC center on 26 August and early 27 August. Vertical wind shear within the 700–500-hPa layer, observable only with more detailed analyses, i.e., hodographs and horizontal plan view plots, likely contributed to this misalignment. Using an idealized modeling framework, Finocchio et al. (2016) similarly demonstrated that greater low-middle tropospheric shear tends to result in increased tilt and more detrimentally impacts TCs than vertical wind shear within other layers. Furthermore, the localized, midtropospheric shear and vortex displacement in Dorian were associated with intrusions of dry air that approached Dorian's inner core and contributed to Dorian's lack of improved organization prior to 27 August.

On 27 August, despite a decrease in the midtropospheric vertical wind shear, vortex misalignment continues with relative humidity asymmetries and a dearth of convection uptilt around 6–12 h before repositioning, which indicates a time-lagged response to the changing environment, a similar finding to an idealized modeling study by Onderlinde and Nolan (2017). Dorian then undergoes a series of events that leads to a modification (preconditioning) of the vortex structure into one that is more conducive for reformation and eventual intensification.

In the six hours prior to the repositioning (0600–1130 UTC 27 August), the LLC broadens, evidenced by the outward radial expansion of the RMW and precipitation, and a decrease in near-center convection, even prior to Dorian's interaction with the islands of St. Lucia and Martinique. This spindown and decrease in convection near the LLC temporally agrees with the TC diurnal cycle, in addition to later observed maxima and minima in stratiform precipitation and convection. Therefore, Dorian may be somewhat analogous to the genesis of Karl (2010; Bell and Montgomery 2019), a storm that featured stratiform-induced humidification (moistening and cooling) positively phased with the diurnal cycle. Bell and Montgomery (2019) hypothesized that the humidification beneficially preconditioned the environment for more persistent convection at later time periods. In addition to its relationships with the diurnal cycle, the precipitation increases shown in Dorian agree with a recent ensemble modeling study (Alvey et al. 2020) and larger satellite composite studies (e.g., Tao and Jiang 2015; Tao et al. 2017) that demonstrated increases in areal coverage of stratiform precipitation just prior to RI onset.

A large increase in deep convection, maximized near the repositioning time (1130–1230 UTC), was observed over and near Martinique, but northeast beyond the center of the MLC. Ultimately, this CB episode led to the formation of multiple mesovortices, one of which reformed into a new, compact low-level vortex between 1200 and 1300 UTC. Embedded within the preexisting, now broadened cyclonic envelope, which included the persistent, broad MLC, the new compact low-level vortex was maintained by episodic convection, predominantly moderate, in the following 12 h.

One of the more unique hypotheses from the study is that Martinique was likely at least partially responsible for

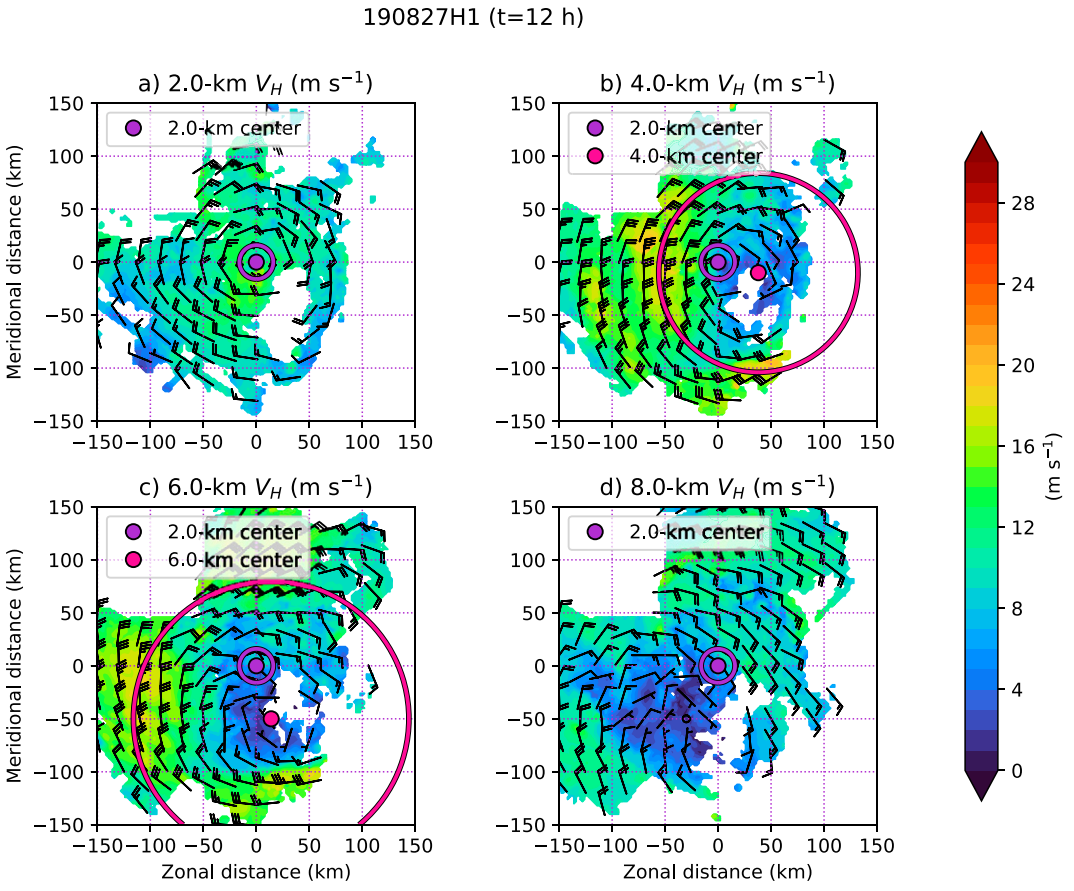

FIG. 14. As in Fig. 3, but for TDR-derived, storm-relative, horizontal wind observed during the 190827H1 mission, approximately 12 h after the center reformation event

invigorating this reformative deep convective burst by providing upstream convergence from enhanced surface friction. In addition to the terrain enhancement, this reformation is a bit unusual from previous documented literature (Nguyen and Molinari 2015; Chen et al. 2018) in that the LLC does not reform directly beneath the center of the preexisting broad MLC that persists in a misaligned configuration even 12–36 h after reformation. It is speculated that the MLC was maintained by robust, persistent stratiform precipitation and its broad kinematic structure supported an environment with greater RH values that allowed the embedded, small reformed vortex to persist in the low levels. Furthermore, the vertical wind shear had relatively weak magnitudes throughout the repositioning period, similar to Schecter and Menelaou's (2020) shear-free idealized modeling study that examines alignment processes.

Factors contributing to the reformation likely included the initial parent vortex's broad structure, and terrain-enhancement of deep convection over Martinique within a more humid environment. The last hypothesized factor, perhaps being the most important, likely led to RI: The new low-level vortex reforms in a moister, favorable environment that is farther removed from midtropospheric dry air that entrained into Dorian's vortex 24 h prior. Although Dorian's intensity, at least defined by maximum sustained winds, only increases slightly in the ensuing 12 h, *the reformation promotes improvement in Dorian's structural organization, ultimately priming the storm for RI* on 28 August and beyond.

Despite maintaining some misalignment (~50 km, 2–6-km tilt) after reformation, Dorian underwent a period of rapid intensification (25 kt in 24 h), during which the vortex became more aligned. Although misalignment likely limited potential intensification rates from greatly exceeding this low-end RI threshold, this also indicates that an *aligned vortex is not required to initiate RI and the TC's alignment can improve during intensification* provided it has a favorable environment and misalignment does not exceed the scale of the vortex (Schecter and Menelaou 2020). Aided primarily by episodic moderate and deep convection, the vortex developed vertically within the misaligned configuration following reformation, likely through contributions from vorticity stretching, tilting, and vertical advection (Chen et al. 2018; Alvey et al. 2020; Rogers et al. 2020).

Center repositioning events like this case's reformation may be more likely than precession for weaker vortices. Although the reformation itself may not have resulted in

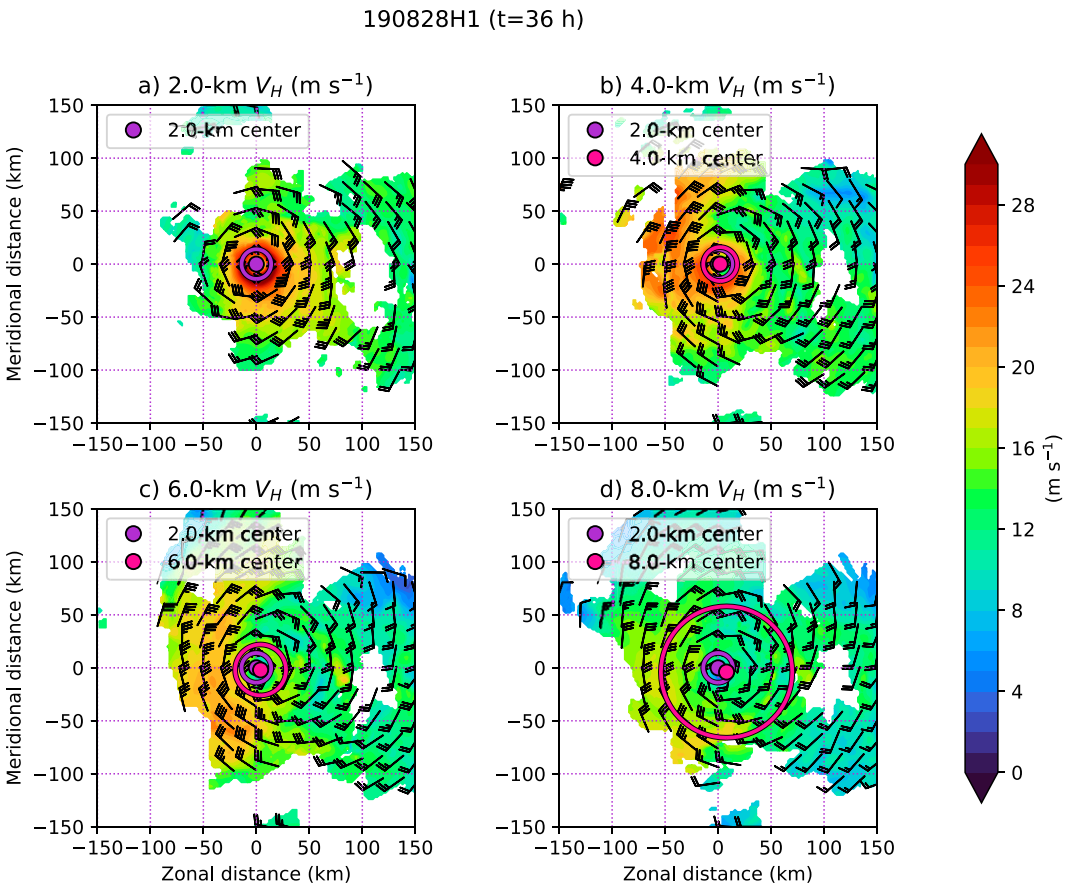

FIG. 15. As in Fig. 3 but for TDR-derived, storm-relative, horizontal wind observed during the 190828H1 mission, approximately 36 h after the center reformation event.

instantaneous alignment in this case, at the very least it likely served as an important precursor step that ultimately facilitated alignment and intensification. For one, the downtilt quadrants tended to have a more humid environment, aided by preexisting precipitation in those quadrants. This places the reformed LLC in a more favorable environment with a greater separation from potentially detrimental dry, midtropospheric air often found in the uptilt (typically upshear) quadrants.

Moving forward, although it may seem intuitively obvious, the authors recommend accounting for not only the current and future environments a TC is moving toward, but also the previous shear and thermodynamic environment the incipient vortex developed in, since its structure will invariably have some imprint from its past that can affect its evolution. We also recommend caution when using static vortex tilt magnitude metrics for weak TCs. These stand-alone metrics, as evidenced by Dorian, are not necessarily indicative of favorable or unfavorable TC structural configurations and/or environments given the potential for time-lagged responses. However, tilt metrics can be extremely valuable when accounting for the tilt's temporal evolution and critical details about the vortex structure (e.g., vertical depth, horizontal scale, multiple centers at different levels). This also includes ensuring a correct portrayal of the tilt magnitude relative to the scale of the vortex and varying vertical wind shear layers. And when located within more marginal environments, the interplay between dry air, vertical wind shear's horizontal and vertical distribution, and the vortex's structure must all be accounted for.

Furthermore, an observation of environmental dry air alone is not sufficient to infer detrimental impacts on the TC's core. It requires a pathway by vertical wind shear and/or a misaligned vortex. The identification of dry air, its vertical overlap with vertical shear layers, and its shear-relative position, can give a further indicator of potential for detrimental impacts caused by ventilation (Riemer and Montgomery, 2011; Alland et al. 2021b). Therefore, we recommend that multiplatform tools continue to be developed not only for research purposes but also for real-time operational usage. Techniques applied here and in other recent TC intensification observational (Rogers et al. 2016; Zawislak et al. 2016; Nguyen et al. 2017; Rogers et al. 2020) and ensemble studies (Munsell et al. 2017; Rios-Berrios et al. 2018; Alvey et al. 2020; Hazelton et al. 2021) should leverage TDR, ground radar networks, and other observing platforms. This also

includes advocating for increased sampling during these low predictability early stage TC restructuring events, wherein airborne platforms like TDR can provide invaluable information about the rapidly evolving structural evolution.

Acknowledgments. The authors thank Xiaomin Chen, Andrew Hazelton, and three anonymous reviewers for providing valuable feedback on the manuscript. The authors would also like to thank Météo-France for providing ground radar data and Francis Breame for assistance in decoding the BUFR radar data into a usable format. The authors would further like to thank Levi Cowan for providing an improved vortex removed shear algorithm.

Data availability statement. All ERA5 data used during this research are openly available from the Copernicus Climate Data Store at (10.24381/cds.bd0915c6). Météo-France restricts the public release of radar data; however, data from Martinique and Guadeloupe's ground radars used in this manuscript may be provided upon request. Tail Doppler radar data may be found at (https://www.aoml.noaa.gov/hrd/data_sub/radar.html) or is available upon request in a quality controlled Level 3 format.

REFERENCES

Alland, J. J., B. H. Tang, K. L. Corbosiero, and G. H. Bryan, 2021a: Combined effects of midlevel dry air and vertical wind shear on tropical cyclone development. Part I: Downdraft ventilation. *J. Atmos. Sci.*, **78**, 763–782, https://doi.org/10.1175/JAS-D-20-0054.1.

——, ——, ——, and ——, 2021b: Combined effects of midlevel dry air and vertical wind shear on tropical cyclone development. Part II: Radial ventilation. *J. Atmos. Sci.*, **78**, 783–796, https://doi.org/10.1175/JAS-D-20-0055.1.

Alvey, G. R., III, J. Zawislak, and E. Zipser, 2015: Precipitation properties observed during tropical cyclone intensity change. *Mon. Wea. Rev.*, **143**, 4476–4492, https://doi.org/10.1175/MWR-D-15-0065.1.

——, E. Zipser, and J. Zawislak, 2020: How does Hurricane Edouard (2014) evolve toward symmetry before rapid intensification? A high-resolution ensemble study. *J. Atmos. Sci.*, **77**, 1329–1351, https://doi.org/10.1175/JAS-D-18-0355.1.

Avila, L. A., S. R. Stewart, R. Berg, and A. B. Hagen, 2020: Tropical cyclone report: Hurricane Dorian (24 August–7 September 2019). NHC Tech. Rep. AL052019, 74 pp., https://www.nhc.noaa.gov/data/tcr/AL052019_Dorian.pdf.

Bell, M. M., and M. T. Montgomery, 2010: Sheared deep vortical convection in pre-depression Hagupit during TCS08. *Geophys. Res. Lett.*, **37**, L06802, https://doi.org/10.1029/2009GL042313.

——, and ——, 2019: Mesoscale processes during the genesis of Hurricane Karl (2010). *J. Atmos. Sci.*, **76**, 2235–2255, https://doi.org/10.1175/JAS-D-18-0161.1.

Bender, M. A., R. E. Tuleya, and Y. Kurihara, 1987: A numerical study of the effect of island terrain on tropical cyclones. *Mon. Wea. Rev.*, **115**, 130–155, https://doi.org/10.1175/1520-0493(1987)115<0130:ANSOTE>2.0.CO;2.

Bukunt, B. P., and G. M. Barnes, 2015: The subtropical jet stream delivers the Coup de Grâce to Hurricane Felicia (2009). *Wea. Forecasting*, **30**, 1039–1049, https://doi.org/10.1175/WAF-D-15-0004.1.

Cangialosi, J. P., E. Blake, M. DeMaria, A. Penny, A. Latto, E. Rappaport, and V. Tallapragada, 2020: Recent progress in tropical cyclone intensity forecasting at the National Hurricane Center. *Wea. Forecasting*, **35**, 1913–1922, https://doi.org/10.1175/WAF-D-20-0059.1.

Carrasco, C. A., C. W. Landsea, and Y. Lin, 2014: The influence of tropical cyclone size on its intensification. *Wea. Forecasting*, **29**, 582–590, https://doi.org/10.1175/WAF-D-13-00092.1.

Chen, D. Y.-C., K. K. W. Cheung, and C.-S. Lee, 2011: Some implications of core regime wind structures in western North Pacific tropical cyclones. *Wea. Forecasting*, **26**, 61–75, https://doi.org/10.1175/2010WAF2222420.1.

Chen, X., Y. Wang, J. Fang, and M. Xue, 2018: A numerical study on rapid intensification of Typhoon Vicente (2012) in the South China Sea. Part II: Roles of inner-core processes. *J. Atmos. Sci.*, **75**, 235–255, https://doi.org/10.1175/JAS-D-17-0129.1.

——, J. A. Zhang, and F. D. Marks, 2019: A thermodynamic pathway leading to rapid intensification of tropical cyclones in shear. *Geophys. Res. Lett.*, **46**, 9241–9251, https://doi.org/10.1029/2019GL083667.

DeMaria, M., and J. Kaplan, 1994: A Statistical Hurricane Intensity Prediction Scheme (SHIPS) for the Atlantic basin. *Wea. Forecasting*, **9**, 209–220, https://doi.org/10.1175/1520-0434(1994)009<0209:ASHIPS>2.0.CO;2.

——, C. R. Sampson, J. A. Knaff, and K. D. Musgrave, 2014: Is tropical cyclone intensity guidance improving? *Bull. Amer. Meteor. Soc.*, **95**, 387–398, https://doi.org/10.1175/BAMS-D-12-00240.1.

Didlake, A. C., Jr., and R. A. Houze Jr., 2013: Dynamics of the stratiform sector of a tropical cyclone rainband. *J. Atmos. Sci.*, **70**, 1891–1911, https://doi.org/10.1175/JAS-D-12-0245.1.

Dunion, J. P., C. D. Thorncroft, and C. S. Velden, 2014: The tropical cyclone diurnal cycle of mature hurricanes. *Mon. Wea. Rev.*, **142**, 3900–3919, https://doi.org/10.1175/MWR-D-13-00191.1.

Finocchio, P. M., S. J. Majumdar, D. S. Nolan, and M. Iskandarani, 2016: Idealized tropical cyclone responses to the height and depth of environmental vertical wind shear. *Mon. Wea. Rev.*, **144**, 2155–2175, https://doi.org/10.1175/MWR-D-15-0320.1.

Fischer, M. S., R. F. Rogers, and P. D. Reasor, 2021: Relationships between vortex tilt, convective structure, and intensity change in early-stage tropical cyclones. *34th Conf. on Hurricanes and Tropical Meteorology*, virtual, Amer. Meteor. Soc., 5B.6, https://ams.confex.com/ams/34HURR/meetingapp.cgi/Paper/373691.

Frank, W. M., and E. A. Ritchie, 2001: Effects of vertical wind shear on the intensity and structure of numerically simulated hurricanes. *Mon. Wea. Rev.*, **129**, 2249–2269, https://doi.org/10.1175/1520-0493(2001)129<2249:EOVWSO>2.0.CO;2.

Gamache, J. F., 1997: Evaluation of a fully three-dimensional variational Doppler analysis technique. Preprints, *28th Conf. on Radar Meteorology*, Austin, TX, Amer. Meteor. Soc., 422–423.

Hazelton, A., G. J. Alaka Jr., L. Cowan, M. Fischer, and S. Gopalakrishnan, 2021: Understanding the processes causing the early intensification of Hurricane Dorian through an ensemble of the Hurricane Analysis and Forecast System (HAFS). *Atmosphere*, **12**, 93, https://doi.org/10.3390/atmos12010093.

Hence, D. A., and R. A. Houze Jr., 2011: Vertical structure of hurricane eyewalls as seen by the TRMM Precipitation

Radar. *J. Atmos. Sci.*, **68**, 1637–1652, https://doi.org/10.1175/2011JAS3578.1.

Hendricks, E. A., M. S. Peng, B. Fu, and T. Li, 2010: Quantifying environmental control on tropical cyclone intensity change. *Mon. Wea. Rev.*, **138**, 3243–3271, https://doi.org/10.1175/2010MWR3185.1.

Hersbach, H., and Coauthors, 2020: The ERA5 global reanalysis. *Quart. J. Roy. Meteor. Soc.*, **146**, 1999–2049, https://doi.org/10.1002/qj.3803.

Houze, R. A., Jr., 2004: Mesoscale convective systems. *Rev. Geophys.*, **42**, RG4003, https://doi.org/10.1029/2004RG000150.

——, 2010: Clouds in tropical cyclones. *Mon. Wea. Rev.*, **138**, 293–344, https://doi.org/10.1175/2009MWR2989.1.

——, W. Lee, and M. M. Bell, 2009: Convective contribution to the genesis of Hurricane Ophelia (2005). *Mon. Wea. Rev.*, **137**, 2778–2800, https://doi.org/10.1175/2009MWR2727.1.

Jones, S. C., 1995: The evolution of vortices in vertical shear. I: Initially barotropic vortices. *Quart. J. Roy. Meteor. Soc.*, **121**, 821–851, https://doi.org/10.1002/qj.49712152406.

——, 2000: The evolution of vortices in vertical shear. II: Large-scale asymmetries. *Quart. J. Roy. Meteor. Soc.*, **126**, 3137–3159, https://doi.org/10.1002/qj.49712657008.

Kaplan, J., and M. DeMaria, 2003: Large-scale characteristics of rapidly intensifying tropical cyclones in the North Atlantic basin. *Wea. Forecasting*, **18**, 1093–1108, https://doi.org/10.1175/1520-0434(2003)018<1093:LCORIT>2.0.CO;2.

——, ——, and J. A. Knaff, 2010: A revised tropical cyclone rapid intensification index for the Atlantic and eastern North Pacific basins. *Wea. Forecasting*, **25**, 220–241, https://doi.org/10.1175/2009WAF2222280.1.

Lee, W.-C., B. J.-D. Jou, P.-L. Chang, and S.-M. Deng, 1999: Tropical cyclone kinematic structure retrieved from single-Doppler radar observations. Part I: Interpretation of Doppler velocity patterns and the GBVTD technique. *Mon. Wea. Rev.*, **127**, 2419–2439, https://doi.org/10.1175/1520-0493(1999)127<2419:TCKSRF>2.0.CO;2.

Leighton, H., S. Gopalakrishnan, J. A. Zhang, R. F. Rogers, Z. Zhang, and V. Tallapragada, 2018: Azimuthal distribution of deep convection, environmental factors, and tropical cyclone rapid intensification: A perspective from HWRF ensemble forecasts of Hurricane Edouard (2014). *J. Atmos. Sci.*, **75**, 275–295, https://doi.org/10.1175/JAS-D-17-0171.1.

Lin, Y., D. B. Ensley, S. Chiao, and C. Huang, 2002: Orographic influences on rainfall and track deflection associated with the passage of a tropical cyclone. *Mon. Wea. Rev.*, **130**, 2929–2950, https://doi.org/10.1175/1520-0493(2002)130<2929:OIORAT>2.0.CO;2.

Mitchell, E. D., S. V. Vasiloff, G. J. Stumpf, A. Witt, M. D. Eilts, J. T. Johnson, and K. W. Thomas, 1998: The National Severe Storms Laboratory tornado detection algorithm. *Wea. Forecasting*, **13**, 352–366, https://doi.org/10.1175/1520-0434(1998)013<0352:TNSSLT>2.0.CO;2.

Munsell, E. B., F. Zhang, J. A. Sippel, S. A. Braun, and Y. Weng, 2017: Dynamics and predictability of the intensification of Hurricane Edouard (2014). *J. Atmos. Sci.*, **74**, 573–595, https://doi.org/10.1175/JAS-D-16-0018.1.

Nguyen, L. T., and J. Molinari, 2015: Simulation of the downshear reformation of a tropical cyclone. *J. Atmos. Sci.*, **72**, 4529–4551, https://doi.org/10.1175/JAS-D-15-0036.1.

——, R. F. Rogers, and P. D. Reasor, 2017: Thermodynamic and kinematic influences on precipitation symmetry in sheared tropical cyclones: Bertha and Cristobal (2014). *Mon. Wea. Rev.*, **145**, 4423–4446, https://doi.org/10.1175/MWR-D-17-0073.1.

——, R. Rogers, J. Zawislak, and J. A. Zhang, 2019: Assessing the influence of convective downdrafts and surface enthalpy fluxes on tropical cyclone intensity change in moderate vertical wind shear. *Mon. Wea. Rev.*, **147**, 3519–3534, https://doi.org/10.1175/MWR-D-18-0461.1.

Onderlinde, M. J., and D. S. Nolan, 2014: Environmental helicity and its effects on development and intensification of tropical cyclones. *J. Atmos. Sci.*, **71**, 4308–4320, https://doi.org/10.1175/JAS-D-14-0085.1.

——, and ——, 2017: The tropical cyclone response to changing wind shear using the method of time-varying point-downscaling. *J. Adv. Model. Earth Syst.*, **9**, 908–931, https://doi.org/10.1002/2016MS000796.

Raymond, D. J., and S. L. Sessions, 2007: Evolution of convection during tropical cyclogenesis. *Geophys. Res. Lett.*, **34**, L06811, https://doi.org/10.1029/2006GL028607.

Reasor, P. D., M. T. Montgomery, and L. D. Grasso, 2004: A new look at the problem of tropical cyclones in vertical shear flow: Vortex resiliency. *J. Atmos. Sci.*, **61**, 3–22, https://doi.org/10.1175/1520-0469(2004)061<0003:ANLATP>2.0.CO;2.

——, ——, and L. F. Bosart, 2005: Mesoscale observations of the genesis of Hurricane Dolly (1996). *J. Atmos. Sci.*, **62**, 3151–3171, https://doi.org/10.1175/JAS3540.1.

——, M. D. Eastin, and J. F. Gamache, 2009: Rapidly intensifying Hurricane Guillermo (1997). Part I: Low-wavenumber structure and evolution. *Mon. Wea. Rev.*, **137**, 603–631, https://doi.org/10.1175/2008MWR2487.1.

——, R. Rogers, and S. Lorsolo, 2013: Environmental flow impacts on tropical cyclone structure diagnosed from airborne Doppler radar composites. *Mon. Wea. Rev.*, **141**, 2949–2969, https://doi.org/10.1175/MWR-D-12-00334.1.

Riemer, M., and M. T. Montgomery, 2011: Simple kinematic models for the environmental interaction of tropical cyclones in vertical wind shear. *Atmos. Chem. Phys.*, **11**, 9395–9414, https://doi.org/10.5194/acp-11-9395-2011.

——, ——, and M. E. Nicholls, 2010: A new paradigm for intensity modification of tropical cyclones: Thermodynamic impact of vertical wind shear on the inflow layer. *Atmos. Chem. Phys.*, **10**, 3163–3188, https://doi.org/10.5194/acp-10-3163-2010.

Rios-Berrios, R., 2020: Impacts of radiation and cold pools on the intensity and vortex tilt of weak tropical cyclones interacting with vertical wind shear. *J. Atmos. Sci.*, **77**, 669–689, https://doi.org/10.1175/JAS-D-19-0159.1.

——, R. D. Torn, and C. A. Davis, 2016: An ensemble approach to investigate tropical cyclone intensification in sheared environments. Part I: Katia (2011). *J. Atmos. Sci.,* **73**, 71–93, https://doi.org/10.1175/JAS-D-15-0052.1.

——, C. A. Davis, and R. D. Torn, 2018: A hypothesis for the intensification of tropical cyclones under moderate vertical wind shear. *J. Atmos. Sci.*, **75**, 4149–4173, https://doi.org/10.1175/JAS-D-18-0070.1.

Rogers, R. F., S. Lorsolo, P. Reasor, J. Gamache, and F. Marks, 2012: Multiscale analysis of tropical cyclone kinematic structure from airborne Doppler radar composites. *Mon. Wea. Rev.*, **140**, 77–99, https://doi.org/10.1175/MWR-D-10-05075.1.

——, P. Reasor, and S. Lorsolo, 2013: Airborne Doppler observations of the inner-core structural differences between intensifying and steady-state tropical cyclones. *Mon. Wea. Rev.*, **141**, 2970–2991, https://doi.org/10.1175/MWR-D-12-00357.1.

——, J. A. Zhang, J. Zawislak, H. Jiang, G. R. Alvey, E. J. Zipser, and S. N. Stevenson, 2016: Observations of the

structure and evolution of Hurricane Edouard (2014) during intensity change. Part II: Kinematic structure and the distribution of deep convection. *Mon. Wea. Rev.*, **144**, 3355–3376, https://doi.org/10.1175/MWR-D-16-0017.1.

——, P. D. Reasor, J. A. Zawislak, and L. T. Nguyen, 2020: Precipitation processes and vortex alignment during the intensification of a weak tropical cyclone in moderate vertical shear. *Mon. Wea. Rev.*, **148**, 1899–1929, https://doi.org/10.1175/MWR-D-19-0315.1.

Ryglicki, D. R., J. D. Doyle, D. Hodyss, J. H. Cossuth, Y. Jin, K. C. Viner, and J. M. Schmidt, 2019: The unexpected rapid intensification of tropical cyclones in moderate vertical wind shear. Part III: Outflow–environment interaction. *Mon. Wea. Rev.*, **147**, 2919–2940, https://doi.org/10.1175/MWR-D-18-0370.1.

Schecter, D. A., and K. Menelaou, 2020: Development of a misaligned tropical cyclone. *J. Atmos. Sci.*, **77**, 79–111, https://doi.org/10.1175/JAS-D-19-0074.1.

Schubert, W. H., and J. J. Hack, 1982: Inertial stability and tropical cyclone development. *J. Atmos. Sci.*, **39**, 1687–1697, https://doi.org/10.1175/1520-0469(1982)039<1687:ISATCD>2.0.CO;2.

Smith, T. M., and K. L. Elmore, 2004: The use of radial velocity derivatives to diagnose rotation and divergence. Preprints, *11th Conf. on Aviation, Range and Aerospace*, Hyannis, MA, Amer. Meteor. Soc., P5.6.

Steiner, M., R. A. Houze, and S. E. Yuter, 1995: Climatological characterization of three-dimensional storm structure from operational radar and rain gauge data. *J. Appl. Meteor.*, **34**, 1978–2007, https://doi.org/10.1175/1520-0450(1995)034<1978:CCOTDS>2.0.CO;2.

Stewart, S., 2019: AL05 Forecast Advisory: Tropical Storm Dorian Discussion 13. National Hurricane Center, accessed 1 November 2020, https://www.nhc.noaa.gov/archive/2019/al05/al052019.discus.013.shtml.

Tang, B., and K. Emanuel, 2010: Midlevel ventilation's constraint on tropical cyclone intensity. *J. Atmos. Sci.*, **67**, 1817–1830, https://doi.org/10.1175/2010JAS3318.1.

——, and ——, 2012: Sensitivity of tropical cyclone intensity to ventilation in an axisymmetric model. *J. Atmos. Sci.*, **69**, 2394–2413, https://doi.org/10.1175/JAS-D-11-0232.1.

Tao, C., and H. Jiang, 2015: Distributions of shallow to very deep precipitation–convection in rapidly intensifying tropical cyclones. *J. Climate*, **28**, 8791–8824, https://doi.org/10.1175/JCLI-D-14-00448.1.

——, ——, and J. Zawislak, 2017: The relative importance of stratiform and convective rainfall in rapidly intensifying tropical cyclones. *Mon. Wea. Rev.*, **145**, 795–809, https://doi.org/10.1175/MWR-D-16-0316.1.

Wang, S., and A. H. Sobel, 2017: Factors controlling rain on small tropical islands: Diurnal cycle, large-scale wind speed, and topography. *J. Atmos. Sci.*, **74**, 3515–3532, https://doi.org/10.1175/JAS-D-16-0344.1.

Wang, X., and H. Jiang, 2021: Contrasting behaviors between the rapidly intensifying and slowly intensifying tropical cyclones in the North Atlantic and eastern Pacific basins. *J. Climate*, **34**, 987–1003, https://doi.org/10.1175/JCLI-D-19-0908.1.

Willoughby, H. E., F. D. Marks, and R. J. Feinberg, 1984: Stationary and moving convective bands in hurricanes. *J. Atmos. Sci.*, **41**, 3189–3211, https://doi.org/10.1175/1520-0469(1984)041<3189:SAMCBI>2.0.CO;2.

Zagrodnik, J. P., and H. Jiang, 2014: Rainfall, convection, and latent heating distributions in rapidly intensifying tropical cyclones. *J. Atmos. Sci.*, **71**, 2789–2809, https://doi.org/10.1175/JAS-D-13-0314.1.

Zawislak, J., H. Jiang, G. R. Alvey III, E. J. Zipser, R. F. Rogers, J. A. Zhang, and S. N. Stevenson, 2016: Observations of the structure and evolution of Hurricane Edouard (2014) during intensity change. Part I: Relationship between the thermodynamic structure and precipitation. *Mon. Wea. Rev.*, **144**, 3333–3354, https://doi.org/10.1175/MWR-D-16-0018.1.

Zhang, F., and D. Tao, 2013: Effects of vertical wind shear on the predictability of tropical cyclones. *J. Atmos. Sci.*, **70**, 975–983, https://doi.org/10.1175/JAS-D-12-0133.1.